Sedimentologika

Research article

Submarine crevasse lobes controlled by lateral slope failure in tectonically-active settings: an exhumed example from the Eocene Aínsa depocentre (Spain)

Ander Martinez-Doñate[1,2*], Euan L. Soutter[1], Ian A. Kane[1], Miquel Poyatos-Moré[3], David M. Hodgson[4], Ashley J. M. Ayckbourne[1], William J. Taylor[4], Max J. Bouwmeester[1], Stephen S. Flint[1]

1 Department of Earth and Environmental Sciences, University of Manchester, Manchester M13 9PL, UK
2 Bureau of Economic Geology, Jackson School of Geosciences, The University of Texas at Austin, Austin, Texas
3 Departament de Geologia, Universitat Autònoma de Barcelona, 08193 Cerdanyola del Vallés, Spain
4 School of Earth and Environment, University of Leeds, Leeds LS29JT, UK

*corresponding author: Ander Martinez-Doñate (ander.martinez-donate@beg.utexas.edu)

doi:10.57035/journals/sdk.2023.e11.1068

Editors: Suzanne Bull and Julien Bailleul
Reviewers: Roberto Tinterri and Rosanna Maniscalco
Copyediting, layout and production: Romain Vaucher, Rachelle Kernen and Faizan Sabir

Submitted: 20.01.2023
Accepted: 17.07.2023
Published: 23.08.2023

Abstract | Tectonic deformation and associated submarine slope failures modify seafloor relief, influencing sediment dispersal patterns and the resulting depositional architecture of deep-water systems. The exhumed Middle Eocene strata of the Banastón deep-water system in the Aínsa depocentre, Spain, allow the interplay between submarine slope confined systems, mass flow deposits, and syn-depositional compressional tectonics to be investigated. This study focuses on the Banastón II sub-unit, interpreted as deposits of low-sinuosity and narrow (2-3 km wide) channel-belts confined laterally by tectonically-controlled, fine-grained slopes. The studied succession (111 m-thick) is exposed along a 1.5 km long SE-NW trending depositional dip section and is documented here by facies analysis and physical correlation of 10 measured sections. Results show a stratigraphic evolution in which the channel axes migrated to the southwest, away from a growing structure in the northeastern part of the Aínsa depocentre. Uplift of this structure promoted the breaching of confining channel walls and slope material with mass failures and the development of sand-rich crevasse scour-fills and crevasse lobes. We show that crevasse deposits form an important component of overbank succession. These crevasse lobes are characterized by structureless thick and medium beds that form < 5 m thick packages in proximal parts and thin abruptly over 1 km across strike (NE) and along downdip (NW) into structured thin beds, similar to the heterolithic dominated overbank deposits. Although the development of crevasse lobes has been observed in multiple deep-water systems in ancient and modern systems, this study documents, for the first time, crevasse lobe development on the active compressional margin of a foreland basin rather than on the opposing, more stable and gentler inactive margin. We discuss the mechanism for forming these crevasse deposits, which exploited the accommodation generated by submarine landslides derived from the tectonically-active compressional margin.

Lay summary | The study examines 111-m thick exhumed Middle Eocene strata of the Banastón deep-water system, focusing on the response of submarine slope channel systems to syn-depositional compressional tectonics. Structural uplift promoted the breaching of confining channel walls and slope material with mass failures, the development of sand-rich crevasse scour-fills and crevasse lobes, and the migration of channel axes away from the growing structure. The dataset includes detailed facies analysis and lithostratigraphic correlation of 10 measured sections along a 1.5 km outcrop belt, which is helpful to reduce uncertainty in subsurface exploration due to variable resolution of seismic reflection data and core/well coverage.

Keywords: Submarine channel, Ainsa, Deep-marine, Crevasse lobes, Submarine landslide, Active margin

1. Introduction

Submarine slope canyons and channel systems are conduits for the delivery of sediment (Mutti and Normark, 1991; Piper and Normark, 2001), nutrients (Heezen et al., 1955), and pollutants (Kane and Clare, 2019; Zhong and Peng, 2021) to deep-water. Submarine channel belts result from erosional degradation of the slope and/or aggradation of constructional overbank deposits (Buffington, 1952; Menard, 1955; Normark, 1970). Sediment-gravity-flows travelling downslope are partially confined within channels, with the more dilute and finer fraction of flows spilling and depositing onto overbank areas (Piper and Normark, 1983; Peakall et al., 2000; Keevil et al., 2006; Kane et al., 2007; Kane and Hodgson, 2011; Hansen et al., 2017a). When these flows are partly unconfined, wedge-shaped external levees are constructed and provide channel confinement (Buffington, 1952; Kane and Hodgson, 2011). However, limited accommodation in confined depocentres, such as in peripheral foreland basins like the Aínsa Basin, hinders the construction of external levees and instead may lead to the development of confined overbank wedges or depositional terraces bounded by the lateral slope(s) (De Ruig and Hubbard, 2006; Hubbard et al., 2009). Breaching of channel margins or external levees can lead to crevasse scours and lobe deposition and can ultimately result in avulsion of the channel (Damuth et al., 1988; Posamentier and Kolla, 2003; Fildani and Normark, 2004; Armitage et al., 2012; Brunt et al., 2013; Maier et al., 2013; Morris et al., 2014a). While the large-scale morphology of structurally confined submarine slope channel systems in the subsurface can be resolved with seismic reflection data, the distribution and decimetre- to metre-scale architecture of sand-prone elements within otherwise mudstone-dominated confined overbank settings are rarely resolvable. In addition, known examples of exhumed crevasse scour-fills and lobes are rare; therefore, their high-resolution sedimentology and stratigraphic architecture are sparsely documented.

Sediment routing systems and deep-water stratigraphic patterns in small, active foreland basins largely depend on the basin physiography, which is often characterised by opposing laterally confining slopes and influenced by the uplift/movement of compressional structures (e.g., Salles et al., 2014; Pinter et al., 2018 and references therein). Submarine channels in these settings are characterised by low sinuosity (Bayliss and Pickering, 2015), and avulsion mechanisms are poorly understood. The longitudinal profile, evolution, and architecture of submarine channels in tectonically-active compressional settings, therefore, tend to be primarily controlled by pre- or syn-depositional tectonic relief (Heiniö and Davies, 2007; Kane et al., 2010a; Tinterri and Muzzi Magalhaes, 2011; Georgiopoulou and Cartwright, 2013; Pinter et al., 2018), halokinesis (Beaubouef and Friedmann, 2000; Gee and Gawthorpe, 2006; Kane et al., 2012) and the emplacement of submarine landslides (Canals et al., 2000; Pickering and Corregidor, 2005; Tinterri and Muzzi Magalhaes, 2011; Fairweather, 2014; Kneller et al., 2016; Kremer et al., 2018; Nwoko et al., 2020; Tek et al., 2020; Steventon et al., 2021; Tek et al., 2021). Hereafter, the term submarine landslide will refer to a remobilized sedimentary body translated downslope due to gravitational instabilities and deposited en masse (Nardin et al., 1979; Hampton et al., 1995; Mulder and Alexander, 2001; Moscardelli and Wood, 2008; Bull et al., 2009; Talling et al., 2012; Kneller et al., 2016).

The exhumed Eocene deep-water strata of the Aínsa Basin show well-preserved examples of submarine slope channel-fill deposits in an active collisional foreland basin setting (Figure 1A). Here, the growth and propagation of structures related to the Pyrenean orogeny controlled the formation and migration of successive deep-water systems (e.g., Pickering and Corregidor, 2005; Arbués et al., 2007; Pickering and Bayliss, 2009; Dakin et al., 2013; Cantalejo and Pickering, 2014; Bayliss and Pickering, 2015; Scotchman et al., 2015; Castelltort et al., 2017; Bell et al., 2018; Tek et al., 2020). This field-based study focuses on the part of the Banastón system (Banastón II sub-unit; Figure 1B) that crops out in the San Vicente area, north of Aínsa (Figure 1C). The Banastón II sub-unit is well-exposed in a 111 m-thick succession along a 1.5 km long depositional dip-oriented (SE-NW) outcrop belt. The objectives of this study are to 1) improve our understanding of the different sub-environments of deposition and architecture of slope channel-fill deposits at bed scale; 2) document the controls and sedimentary processes involved in crevasse lobe development; and 3) evaluate the role that active tectonism and mass-wasting processes played in the evolution and avulsion of the Banastón deep-water system.

2. Geological setting

Late Cretaceous to Miocene convergence between the Eurasian and Iberian continental plates resulted in the formation of the Pyrenees (Srivastava and Roest, 1991; Muñoz, 1992; Muñoz, 2002; Rosenbaum et al., 2002) and their related north and south peripheral foreland basins (Figure 1A). The southern foreland basin is characterised by a southward-verging thin-skinned fold-and-thrust system, which led to the development of a WNW-ESE oriented and westward deepening, narrow and elongated basin, with evolving foredeep to piggyback depocentres (Muñoz, 1992, 2002; Dreyer et al., 1999). Typically, the south-central foreland basin is subdivided into three main sectors, which formed a linked source-to-sink system during the Early to Middle Eocene (Nijman, 1998; Payros et al., 2009; Chanvry et al., 2018): i) the Tremp-Graus depocentre in the east, with alluvial, fluvio-deltaic and shallow-marine deposits; ii) the Aínsa depocentre in the central part, dominated by submarine slope deposits; and iii) the Jaca depocentre in the west, where basin floor deposits are found. The deep-water deposits of the Aínsa and Jaca depocentres are collectively known as the Hecho Group (Mutti et al., 1972) and have been the focus of many studies (e.g., Barnolas and Gil-Peña, 2001; Remacha and Fernández,

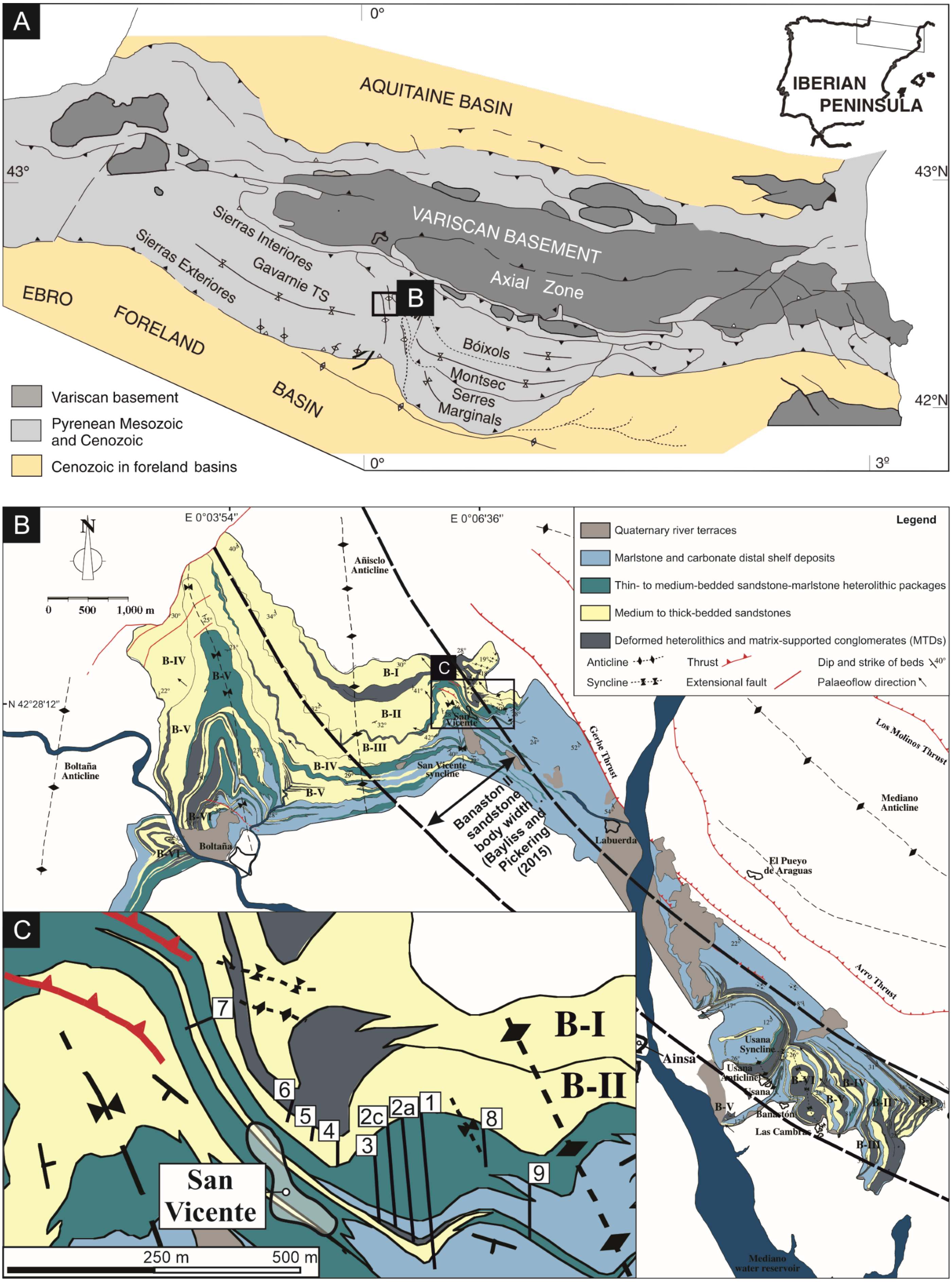

Figure 1 | (A) Structural map of the Pyrenees (after Muñoz et al., 2013) and location of the Aínsa Basin (see black square). (B) Geologic map of the Banastón system and the main structures (after Bayliss and Pickering, 2015). Note the black square indicating the location of the study area. (C) Geologic map of the study area near the San Vicente town (after Pickering and Bayliss, 2009; Bayliss and Pickering, 2015), and the sedimentary logs (1-9) collected in this study.

2003; Pickering and Corregidor, 2005; Arbués et al., 2007; Payros et al., 2009; Pickering and Bayliss, 2009; Clark and Cartwright, 2011; Castelltort et al., 2017). The fluvio-deltaic environments in the east predominantly fed the turbiditic systems of the Hecho Group (Fontana et al., 1989; Gupta and Pickering, 2008; Caja et al., 2010; Thomson et al., 2017), supplying the Aínsa depocentre through a series of tectonically controlled submarine canyons and channel systems (Mutti, 1977; Puigdefàbregas and Souquet, 1986; Millington and Clark, 1995).

In the Aínsa depocentre, seven deep-water systems have been recognized, from older to younger: Fosado, Arro, Gerbe, Banastón, Aínsa, Morillo, and Guaso (Burbank et al., 1992; Payros et al., 2009; Poyatos-Moré, 2014; Bayliss and Pickering, 2015; Scotchman et al., 2015; Castelltort et al., 2017; Clark et al., 2017). This study focuses on the Lutetian-aged Banastón system, which ranges in thickness from ~500 m on the upper slope to ~700 m on the lower slope (Bayliss and Pickering, 2015). The channelised system was characterised by an axial supply (NNW-directed palaeoflow) with a lateral-offset stacking pattern towards the WSW (Figure 1B). The progressive migration of channel axes towards the WSW was controlled by syn-depositional growth and propagation of local NW-SE oriented oblique-lateral ramp structures related to regional E-W thrust sheets (Poblet et al., 1998; Fernández et al., 2012; Muñoz et al., 2013).

Bayliss and Pickering (2015) mapped six channelised sandstone bodies within the Banastón system: Banastón I (BI: 149 m thick and 2000 m wide), Banastón II (BII: 98 m thick and 1800 m wide), Banastón III (BIII: 72 m thick and 1700 m wide), Banastón IV (BIV: 124 m thick and 2500 m wide), Banastón V (BV: 97 m thick and 3300 m wide), and Banastón VI (BVI: 160 m thick and 2400 m wide) (Figure 1B). These six channelised sandstone bodies were grouped into Stage 1 (BI-BIII) and Stage 2 (BIV-BVI) by Bayliss and Pickering (2015), where BI, BII and BIII were confined between the Mediano and Añisclo anticlines, and BIV, BV and BVI between the Añisclo and Boltaña anticlines, forming two NNW-SSE-oriented ~5-8 km wide corridors. This study focuses on the Banastón II sub-unit, whose deposition has been linked to a period of active compressional tectonics in the basin (Läuchli et al., 2021).

3. Data and methods

We investigated the sedimentology and stratigraphic architecture of a 111 m-thick section in the Banastón II sub-unit over a 1.5 km SW-NE oriented outcrop belt. The bedding of strata within the studied succession dips at 30° to the SSW. We measured and described 10 detailed sedimentary logs (Figure 1C) at a 1:20 scale to document bed thickness, lithology, sedimentary structures, textures, and palaeocurrent measurements (n=73) from ripple foresets, flute and groove casts. Sedimentary logs were correlated by walking out individual sandstone packages, enabling the vertical and lateral characterization of different facies associations and the general stratigraphic evolution of the Banastón II system in the study area. Additionally, 7 detailed logs were collected at a 1:2 scale to document specific stratigraphic intervals' complexity and fine-scale thickness variability. The sandstone-mudstone proportion was analysed and plotted using the Striplog Python package (https://github.com/agile-geoscience/striplog). Additionally, Uncrewed Aerial Vehicle (UAV) photogrammetric models were built to capture the stratigraphic architecture of stratal packages in inaccessible areas.

4. Facies associations

Based on facies and outcrop analysis, we recognised 14 lithofacies in the Banastón II sub-unit (Figures 2, 3, 4, Tables 1 and 2). These lithofacies have been grouped into 5 facies associations (Figure 5), representing different depositional sub-environments.

4.1. FA1: Overbank deposits

Description: This facies association is characterised by thin-bedded heterolithic < 20 m thick successions (Figure 5A) dominated by alternating structureless carbonate mudstones (Lf1) and thin-bedded siltstones and sandstones (Figure 2A). Some thin siltstone and sandstone beds have flat to loaded bases and lenticular geometries and may pinch out laterally (Lf2a) or are laterally extensive (Lf2b) over tens of metres (Figure 2A and Figure 2B). Lf2a is structureless or comprises starved-ripple cross-lamination (Figure 2A), indicating NW-directed palaeoflows, while Lf2b shows planar lamination (Figure 2B). Locally, the conformable bedding of FA1 can be interrupted by unconformable 0.5-7 m thick deformed thin-bedded packages rotated above south-westwards dipping concave-up planes (Lf7a and Lf7b; Figures 4A-4C). Lf7a is thinner than 5 m and shows limited disaggregation, with minor deformation in the bedding (Figures 4A and 4B). However, Lf7b is 5-7 m thick, and the bedding is deformed and comprises metre-scale fold amplitudes (Figure 4C).

Interpretation: The development of FA1 is the result of combined deposition from dominantly background sedimentation and low-density fine-grained turbidity currents. Here, background sedimentation refers to hemipelagic settling and thin dilute sediment gravity flow deposits not visible to the naked eye in outcrop (Boulesteix et al., 2019, 2020, 2022). These accumulations of thin beds are interpreted as the product of flow-stripping of the dilute upper parts of channelised turbidity currents into the overbank areas (Piper and Normark, 1983; Peakall et al., 2000; Keevil et al., 2006; Kane et al., 2007; Kane and Hodgson, 2011; Hansen et al., 2017a). When these flows exit the confining channel belt, they are characterised by capacity-driven deposition as they become less confined (Hiscott, 1994a; Hübscher et al., 1997; Posamentier and Kolla, 2003; Kane et al., 2007, 2010b) causing rapid deceleration and the development of transitional behaviour from an initially turbulent flow to more laminar flows (e.g.,

Lithofacies	Lithology	Description	Thickness	Process interpretation	Photo
Lf1: Structureless mudstone	Carbonate mudstone	No grading or other sedimentary structures.	No clear bedding	Deposits from hemipelagic suspension fallout or low-density turbidity currents, which are too fine-grained to differentiate by the naked eye (Boulesteix et al., 2019).	Figure 2A
Lf2a: Lenticular thin-bedded siltstones and sandstones	Siltstone to fine-grained sandstones	Sandstones with flat bases and convex tops. Lenses can be 5-20 cm long.	1-10 cm	Deposition from a partially bypassing flow and reworking by distal, sluggish, and small-volume low-density turbidity current (Allen, 1971, 1982; Jobe et al., 2012).	Figure 2A
Lf2b: Structured thin-bedded sandstones	Very fine to medium-grained sandstone	Normally graded, moderately sorted thin-beds. Fine- to medium-grained bases and (very) fine-grained tops. Planar laminated from base to top.	1-10 cm	Deposition and tractional reworking by steady low-density turbidity current (Allen, 1971).	Figure 2B
Lf3a: Lenticular medium-bedded sandstones	Very fine- to coarse-grained sandstones	Sandstones with flat bases and convex tops. Lenses can be 5-20 m long with 10-40 cm amplitudes. They are structureless at the base, overlain by planar or sinusoidal bedforms. Overlying deposits can onlap onto these sandstone bodies.	0-40 cm	Deposition from unsteady and unidirectional low- to medium-density turbidity currents (Allen, 1973; Kneller, 1995). Convex tops are associated with tractional reworking from bypassing and steady turbidity currents and/or deposition from combined flows (Tinterri, 2011) formed because of the interaction with intrabasinal topography (Pickering and Hiscott, 1985; Kneller et al., 1991).	Figure 2C
Lf3b: Planar laminated argillaceous medium-bedded sandstone	Coarse to fine-grained argillaceous sandstones	Argillaceous sandstones with well-developed planar laminations and wavy tops. The bed bases can be structureless.	10-60 cm	Deposits beneath mud-rich transitional plug flow are formed by steady, unidirectional, and tractional reworking within the upper stage flow regime (Baas et al., 2009, 2011; Baas et al., 2016; Stevenson et al., 2020).	Figure 2D
Lf3c: Climbing-ripple and sinusoidal laminated medium-bedded argillaceous sandstone	Coarse to fine-grained argillaceous sandstones	Bipartite sandstones comprise a sandy basal division passing gradually into the argillaceous division. Alternating structureless and supercritical climbing ripple lamination. Sinusoidal laminations are common near bed tops.	10-50 cm.	Deposition from long-lived surging flows under high-aggradation rates and tractional reworking (Jobe et al., 2012). The flows ultimately collapse, increasing the fallout rate and developing sinusoidal lamination (Tinterri, 2011; Jobe et al., 2012).	Figure 2E
Lf4a: Erosional mudstone clast-rich thick-bedded sandstones.	Coarse to fine-grained argillaceous sandstones	Highly amalgamated, crudely normally graded, and structureless thick-bedded sandstones. Bed tops are silty, locally developing planar laminations towards bed tops. Bed bases are unconformable, with abundant grooves and bioturbation. Mudstone-clast-rich horizons and grain-size breaks are common.	0.5-1.2 m	Deposition under high-density partially bypassing turbidity currents (sensu Lowe, 1982), formed by incremental layer-by-layer deposition with high aggradation rates (Sumner et al., 2008; Talling et al., 2012). Scouring and entrainment of the fine-grained substrate are common.	Figure 2F
Lf4b: Structureless thick-bedded argillaceous sandstones	Coarse to fine-grained argillaceous sandstones	Often amalgamated and structureless thick-bedded sandstones that become gradually argillaceous towards bed tops. Bed bases are mostly conformable; however, not always. Decimetre-scale burrows from top to basal contacts, not limited to bed bases.	0.5-1.2 m	Deposition from high-density turbidity currents (sensu Lowe, 1982) formed by incremental layer-by-layer deposition with high aggradation rates (Kneller and Branney, 1995; Sumner et al., 2008; Talling et al., 2012). The upper argillaceous division reflects the fine-grained tail of the flow, which collapsed due to radial spreading and abrupt loss in flow capacity.	Figures 2G and 2H

Table 1 | Description, process interpretation and photographs of the Lf1 – Lf4b lithofacies.

Lf3b). Rotated stratigraphy is also a common feature of overbank environments adjacent to channels (e.g., Kane et al., 2007; Kane et al., 2011; Dykstra et al., 2007; Hubbard et al., 2009; Hansen et al., 2015) and represents localised submarine landslide deposits of nearby stratigraphy such as from draping and accretion on steep bounding slopes (Abreu et al., 2003; De Ruig and Hubbard, 2006; Hubbard et al., 2009) where the channel belt is confined.

4.2. FA2: Terrace deposits

Description: This facies association is characterized by medium-bedded heterolithic <5 m thick successions (Figure 5B), with a basal matrix-supported conglomerate (Lf7c; Figures 4D and 4E), overlain by an alternation of carbonate mudstone (Lf1; Figure 2A) and thin- to medium-bedded sandstones with a wide grain size range from fine to pebbly sand (Figure 5B). Deformed heterolithic packages rotated above concave-up planes are also observed (Lf7a; Figures 4A and 4B). Some medium-bedded sandstones show rounded, convex-up tops that exhibit positive relief up to 10 cm, which also pinches out laterally over several metres (Lf3a; Figure 2C). This facies association also comprises medium-bedded tabular sandstones with sharp flat bases and sharp wavy tops (Lf3b; Figure 2D). Commonly, Lf3b is structureless at the base, with well-developed planar lamination towards the top. In addition to the lithofacies described above, FA2 is differentiated from FA1 by dune-like lenticular bodies and associated scour surfaces (Soutter et al., 2023). Dune-forming beds are structureless or comprise faintly planar laminated basal divisions that pass vertically into a normally graded well sorted granular to pebbly sandstone division (Lf6; Figures 3C, 3D, and 3E) with well-developed foresets, characterized by abundant mudstone clasts dipping consistently towards the NNW (Figure 3C). Foresets are commonly overlain by a grain size break and a finer-grained ripple laminated division representing the top division (Soutter et al., 2023), indicating NW-directed palaeoflow. Bed tops are characterised by intense bioturbation (Thalassinoides; Figure 3F). Furthermore, Lf6 dune-forming beds exhibit a distinctive reddish colour and, in plan view, develop crescentic-shaped profiles (Figure 3D) (Soutter et al., 2023). Lf6 overlies matrix-supported conglomerate (Lf7c) and becomes less frequent toward the top of the FA2 stratal packages.

Interpretation: The variability in deposit thickness and grain size range in the FA2 deposits suggests an environment of deposition dominated by flows of variable magnitudes (Soutter et al., 2023). The thin-bedded siltstones are interpreted to represent deposition from overspilling and flow stripping of lower magnitude flows (Peakall et al., 2000; Dennielou et al., 2006; Hansen et al., 2015). On the

Lithofacies	Lithology	Description	Thickness	Process interpretation	Photo
Lf5: Sand-filled scour	Argillaceous sandstone bearing abundant mudstone clasts along laminae	Medium- to thick-bedded sandstones with sharp unconformable concave-up (< 1 m) bases and flat tops. This lithofacies is structureless, planar laminated, or dune-scale cross-bedded, bearing abundant mudstone clasts along laminae. Abundant burrows.	0.3-1 m	Deposition from high-density turbidity currents (sensu Lowe, 1982) formed by incremental layer-by-layer deposition with high aggradation rates (Kneller and Branney, 1995; Sumner et al., 2008; Talling et al., 2012). Planar and dune-scale cross-bedding bearing abundant mudstone clasts along the laminae represent deposition from energetic, steady, and partially bypassing flows (Arnott, 2012; Talling et al., 2012; Stevenson et al., 2015).	Figures 3A and 3B
Lf6: Medium-bedded granular sandstones	Medium to granular sandstone with mudstone clasts.	In plan view, medium-bedded granular sandstone with well-developed NW migrating dune-like bedforms with a crescentic shape. The cross-bedding is coarser-grained (granular to pebbly) than the surrounding sandstone (medium to very coarse). Rounded carbonate mudstone clasts are common.	20-50 cm	The abundant mudstone clasts suggest a partially bypassing flow (F6 of Mutti, 1992; Stevenson et al., 2015; Tinterri et al., 2017) that reworked the previously deposited coarse fraction, forming dunes. Dune-like bedforms are attributed to high-magnitude steady parental flow (Arnott, 2012; Talling et al., 2012).	Figures 3C, 3D, 3E and 3F.
Lf7a: Rotated heterolithics	Thin- to medium-bedded heterolithics.	Rotated heterolithic (Lf1, Lf2a, Lf2b) packages are characterised by decimetre-scale low-amplitude sinusoidal folding lacking internal disaggregation. Folding and normal faulting verge SW (perpendicular to palaeoflow and parallel to the SW dipping active margin). The base of the deposit is often marked by a concave-up glide plane. At the top of this package, < 0.3 m thick sandstone beds showing localised thickness changes are common; thickening in the hanging-wall towards the fault when the Lf7a is thinnest and thinning or pinching out when Lf7a is thickest.	0.5-5 m	Local sliding of nearby stratigraphy (not disaggregated). Intraformational and non-erosional. The thickness changes of the top sandstone can be related to the pre-depositional rugosity of the slide (e.g., Armitage et al., 2009) or can be related to syn-depositional creeping/sliding (e.g., Ayckbourne et al., 2023)	Figures 4A and 4B
Lf7b: Folded heterolithics	Thin- to thick-bedded heterolithics.	Deformed heterolithic (Lf1, Lf2a, Lf2b, Lf4a, Lf4b, Lf5, Lf6, Lf7c) package characterised by metre-scale amplitude open to recumbent folding. Normal faults and folds display SW vergence.	5-8 m	Local slumping of nearby stratigraphy (limited disaggregation). Intraformational and non-erosional. Equivalent to Type Ia MTCs of Pickering and Corregidor (2005).	Figure 4C
Lf7c: Matrix-supported conglomerate	Mud rich medium-grained sandstone to sandy mudstone.	Poorly sorted and ungraded with a chaotic distribution of clasts floating in a sandy mudstone matrix. Clasts show bimodal lithology: sub-rounded carbonate clast (> 15 cm) and sub-rounded to elongated sandstone clast (0.15 – 2 m). Irregular and sharp bases can be erosive, undulatory tops.	0.5-7 m	Cohesive debris-flow deposits (sensu Talling et al., 2012). The carbonate clasts are extraformational sediments eroded and reworked prior to their input to deep-water settings, while the sandstone clasts represent the rafting and incorporation of intraformational material into the debris flows. Equivalent to Type II MTCs of Pickering and Corregidor (2005).	Figures 4D and 4E
Lf7d: Sheared mudstone	Carbonate mudstone	Disaggregated and sheared carbonate mudstones, highly bioturbated	0.1-3 m	Local failure of nearby fine-grained stratigraphy. Bioturbation suggests that these deposits were overridden by nutrient- and oxygen-bearing flows and proximity to channels.	Figure 4F

Table 2 | Description, process interpretation and photographs of the Lf5 and Lf6 and Lf7 lithofacies.

other hand, the sandstones and coarse-grained dune-like deposits indicate deposition from steady (Kneller and Branney, 1995) and bypassing high magnitude energetic flows, which reworked a previously deposited coarser fraction (Amy et al., 2000; Stevenson et al., 2015; Hansen et al., 2021). Furthermore, the lack of channel-scale erosional features within these packages suggests that FA2 corresponds to terrace deposits formed on a relatively flat to shallow surface in an elevated position relative to the active channel, yet still inside the channel belt (Babonneau et al., 2002, 2004, 2010; Hansen et al., 2015, 2017a, 2017b; Allen et al., 2022). The basal matrix-supported conglomerates (Lf7c; Figure 5B) are considered local deposits of cohesive debris flows (Talling et al., 2012), which might have created a rugose topographic high, which formed the initial terrace surface. The deformed heterolithic units (Lf7a) are attributed to gravitational failures of the channel walls and/or adjacent confining slopes (Hansen et al., 2015, 2017b; Allen et al., 2022).

4.3. FA3: Channel-fill deposits

Description: FA3 comprises a 5-15 m thick package (Figure 5C) dominated by highly amalgamated thick-bedded sandstones, commonly overlying a basal muddy, matrix-supported, extrabasinal clast-bearing conglomerate (Lf7c; Figures 4D and 4E). The thick sandstone beds are weakly normally graded, commonly structureless, and feature NNW-directed flutes with locally developed planar and NNW-dipping ripple lamination (Lf4a; 2F). In the lower half of FA3, where not amalgamated, the thick beds of Lf4a show silty tops and are bounded by heterolithic packages (<0.3 m) of Lf1 and Lf2b (Figure 5C). In the upper half, they develop unconformable bases that overlie erosion surfaces (up to 0.5 m) into the underlying stratigraphy, with abundant scours, mudstone clasts, and grain-size breaks (Figure 5C).

Interpretation: The basal matrix-supported conglomerates represent deposition from cohesive debris flows. The amalgamation and weak normal grading within thick beds suggest deposition from high-density turbidity currents (sensu Lowe, 1982) under high aggradation rates (Kneller and Branney, 1995; Sumner et al., 2008). Furthermore, the silty tops of the thick beds in the lower half of FA3 suggest an abrupt loss in capacity and competence and deposition under high deceleration rates. In contrast, the scouring, abundance of mudstone clasts, and grain-size breaks reported in the upper half suggest sediment bypass and erosional flows (Stevenson et al., 2015). These stratal packages are therefore interpreted as deposits from channelized flows. However, the lack of major erosional surfaces (at the exposure scale) and minor bypass indicators suggest that FA3 is more closely related

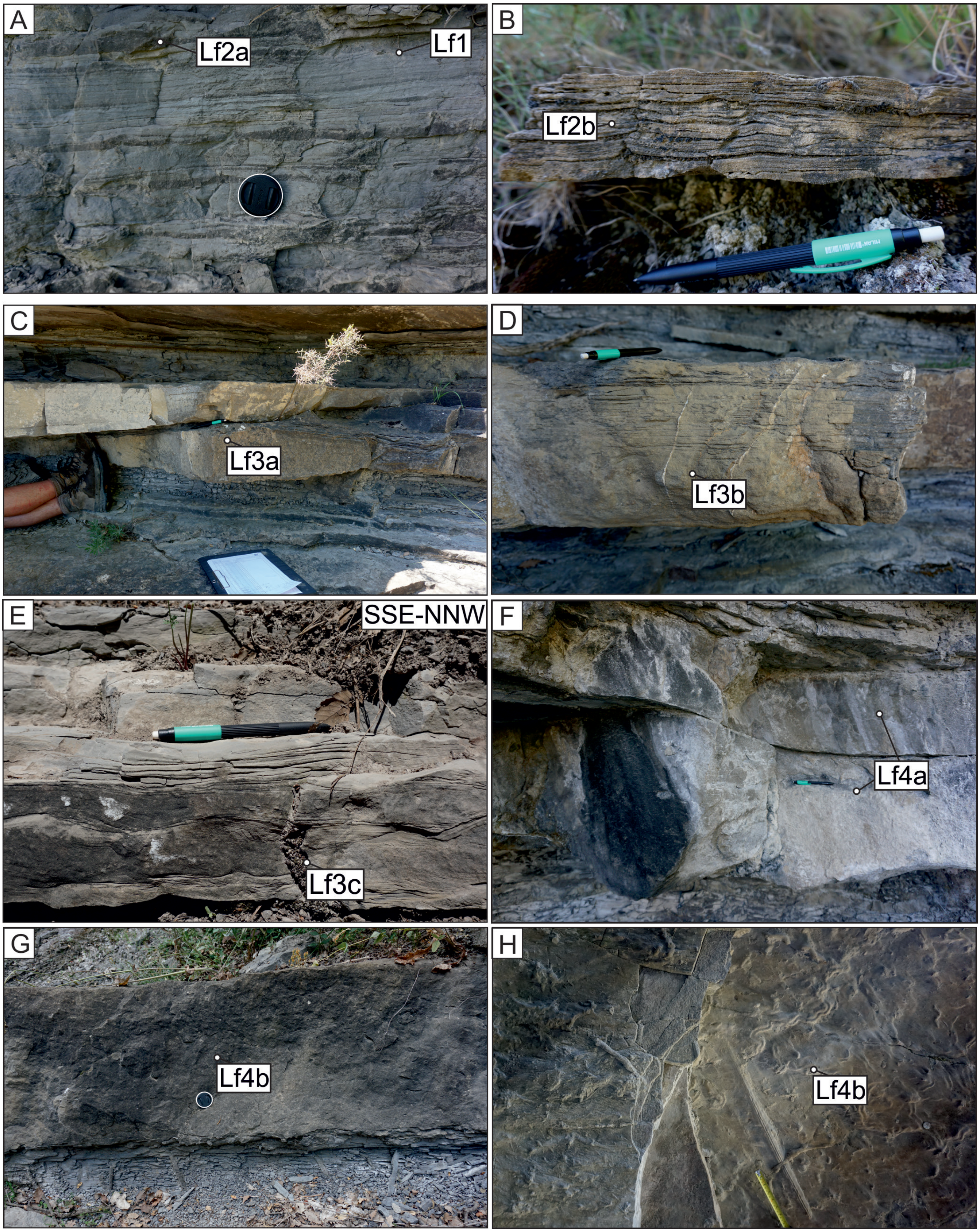

Figure 2 | Representative outcrop photographs of Lf1-Lf4b lithofacies. (A) Thin-bedded, fine-grained heterolithics are characterised by alternating between carbonate mudstone (Lf1) and siltstone to fine-grained sandstone (Lf2a). (B) Thin-bedded planar-laminated sandstone (Lf2b). (C) Lenticular medium-bedded sandstones (Lf3a). Note the onlap of the sandstone bed onto the Lf3a bed due to its positive relief. (D) Planar and ripple-laminated argillaceous medium-bedded sandstone (Lf3b). (E) Climbing-ripple medium-bedded sandstone (Lf3c). (F) Erosional mudstone clast-rich thick-bedded sandstones. Note pencil for scale. (G) Structureless thick-bedded argillaceous sandstones. (H) Base of structureless thick-bedded argillaceous sandstones with abundant bioturbation and groove marks.

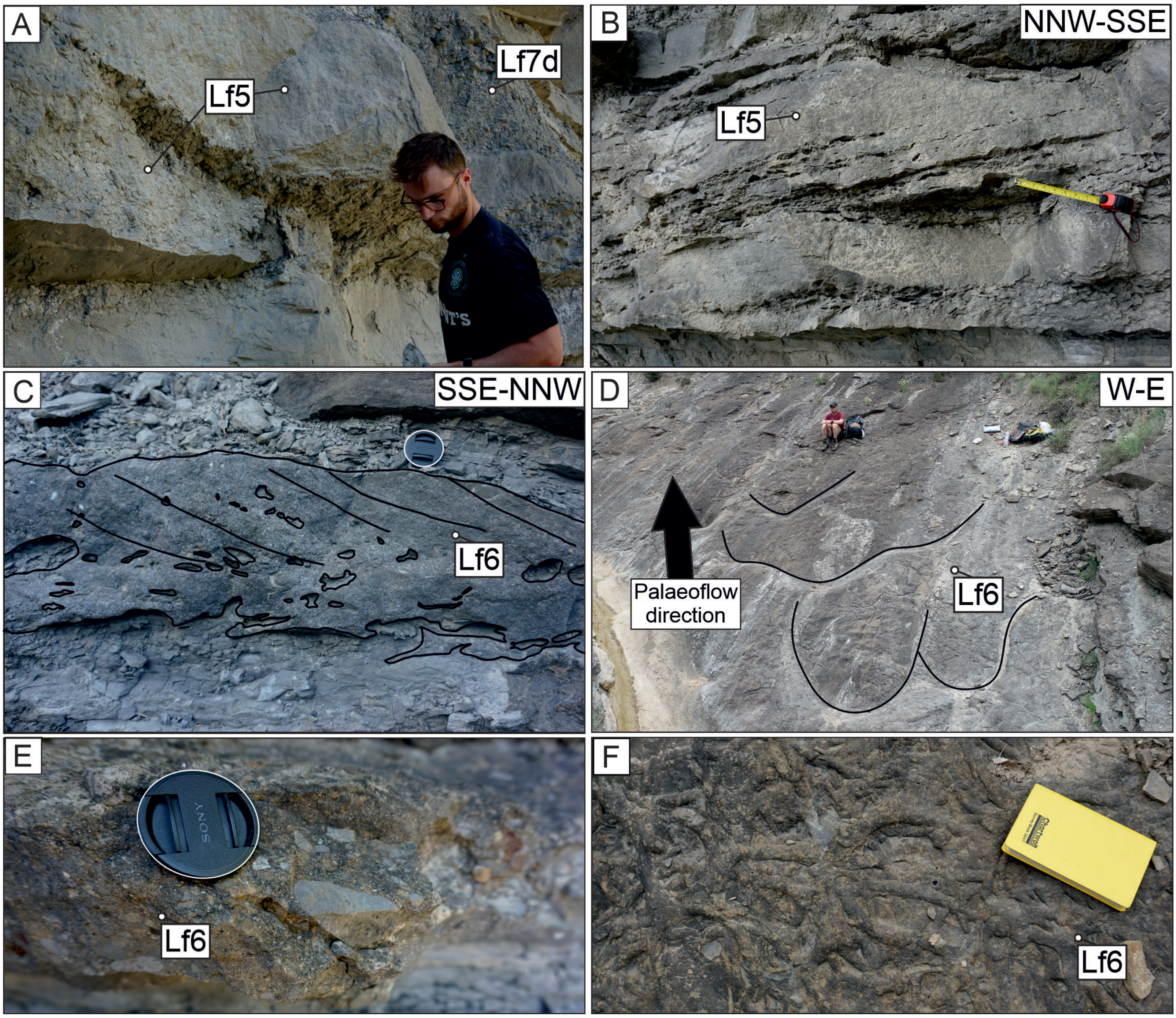

Figure 3 | Outcrop photographs of Lf5 and Lf6 lithofacies. (A) Structureless and (B) dune-scale cross-bedded thick-bedded sandstone scour-fill. Note in (A) the abundant burrows at the scour dipping towards the right hand and in (B) the abundant mudstone clasts along the laminae. (C) Medium-bedded granular sandstone with well-developed NW migrating dune-like bedforms (Lf6). See the lens cap for scale. The cross-bedded fraction is coarser-grained (granular to pebbly) than the surrounding sandstone (medium to very coarse). (D) Plan view of Lf6 showing the crescentic-shaped profiles. See geologist for scale. (E) Very coarse-grained sandstone bearing carbonate mudstone intraclasts. (F) Intensely bioturbated (Thalassinoides) tops of Lf6.

to channel backfilling than being representative of early channel formation, i.e., erosion and almost complete bypass (Hodgson et al., 2016), while the basal surface of the matrix-supported conglomerates (here interpreted as debrites rather than lag deposits) would indicate the base of the channel.

4.4. FA4: Crevasse scour-fill deposits

Description: This facies association comprises a <5 m thick succession (Figure 5D) of highly amalgamated sandstone beds interbedded with sheared mudstone intervals (Lf7d). Medium- to thick-bedded sandstones (Lf5) with poor lateral continuity (<100 m long) and low aspect ratios (5:1 to 10:1, width:thickness) characterise this facies association (Fig3A and Fig3B). Scours bound the base of Lf5 and Lf7d (<2 m thick), truncating underlying beds (Figure 5D). Lf5 sandstone beds are planar or cross-bedded, medium- to coarse-grained with grain-size breaks, comprising abundant mudstone clasts oriented parallel to the laminae and centimetre-scale grooves at bed bases (Figures 3A and 3B). Lf5 sandstone beds comprise grooves with high divergence in contrast to the flutes and the crossbedding, which consistently indicate NNW-oriented palaeoflow. Abundant centimetre- to decimetre-scale burrows are observed, preferentially at the base of the thick-bedded sandstone (Figure 3A) or elongated (5-50 cm long) from top to base at sheared mudstone intervals (Lf7d; Figure 4).

Interpretation: Lf5 sandstone and Lf7d mudstone beds represent small-scale scour-fills (Arnott and Al-Mufti, 2017), while the truncation and low aspect ratio beds observed at their base support scouring of the substrate by previously bypassing flows (Pemberton et al., 2016; Terlaky and Arnott,

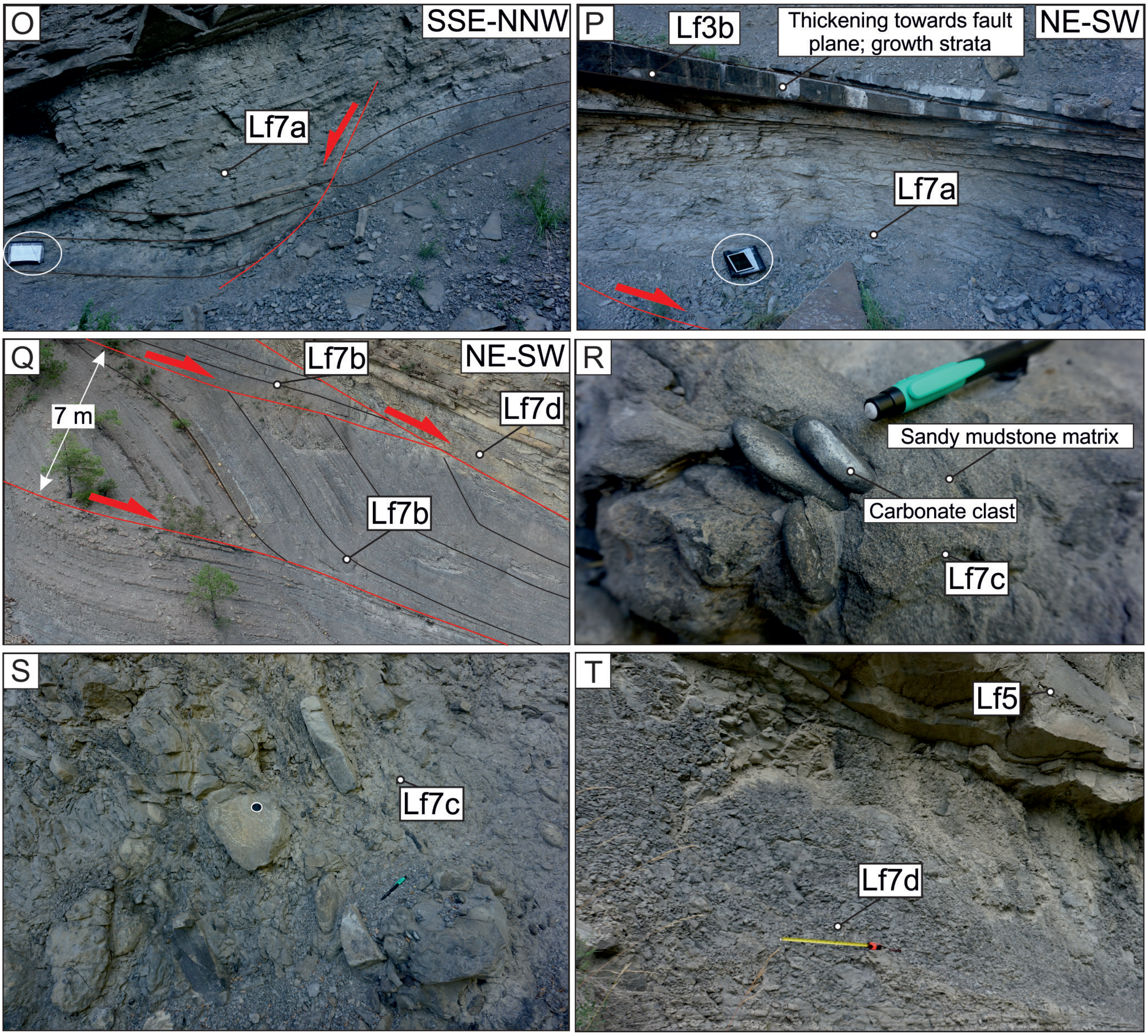

Figure 4 | Outcrop photographs of Lf7a-Lf7d lithofacies. (A) The rotated thin-bedded heterolithic package exhibits minor internal disaggregation (Lf7a) and interpreted as a slide deposit. The base of (Lf7a) is often marked by a concave-up glide plane. (B) At the top of Lf7a, < 0.3 m thick sandstone beds show localised thickening towards the slide plane and pinching away from it (towards the right hand). (C) Deformed heterolithic package characterised by metre-scale amplitude open to recumbent folding (Lf7b) interpreted as slump deposits. Normal faults and folds show SW vergence. (D and E) Matrix-supported poorly sorted and ungraded conglomerate (Lf7c) interpreted as debrites. Clasts show bimodal lithology: (D) sub-rounded carbonate clasts (> 15 cm) and (E) sub-rounded to elongated sandstone clasts (0.15 – 2 m). (F) Disaggregated and sheared carbonate mudstones, which are highly bioturbated (Lf7d), and interpreted as the deposits of the local failure of nearby fine-grained stratigraphy.

2016; Hofstra et al., 2018; Pohl et al., 2020). The deposition of crudely graded to ungraded (Lf5) sandstones over the scour surfaces is interpreted as the product of high sedimentation rates from high-density turbidity currents (sensu Lowe, 1982), suppressing tractional reworking and, therefore, consistent with crevasse-related sedimentation. The development of grain-size breaks, cross-bedding and mudstone clast horizons in Lf5 indicates partial bypass by sustained flows (Kneller and McCaffrey, 2003; Kane et al., 2009; Stevenson et al., 2015). The sheared mudstones (Lf7d) indicate compression along the front of localised, small-scale failures of nearby fine-grained stratigraphy (Ayckbourne et al., 2022). The intense burrowing supports sustained high oxygen and nutrient levels, suggesting proximity to channels.

4.5. FA5: Crevasse lobe deposits

Description: This facies association forms a medium- to thick-bedded tabular sandstone package (1.5–5 m thick; Figure 5E). The dominant lithofacies are thick-bedded, structureless, crudely graded sandstones (Lf4b; Figure 2G). Lf4b is characterised by abundant decimetre-scale burrows and silty tops (Figures 2G and 2H; e.g., Morris et al., 2014a). When not amalgamated, thick beds are bounded by 1-30 cm thick mudstone intervals (Lf1) or thin- to medium-bedded planar laminated sandstones

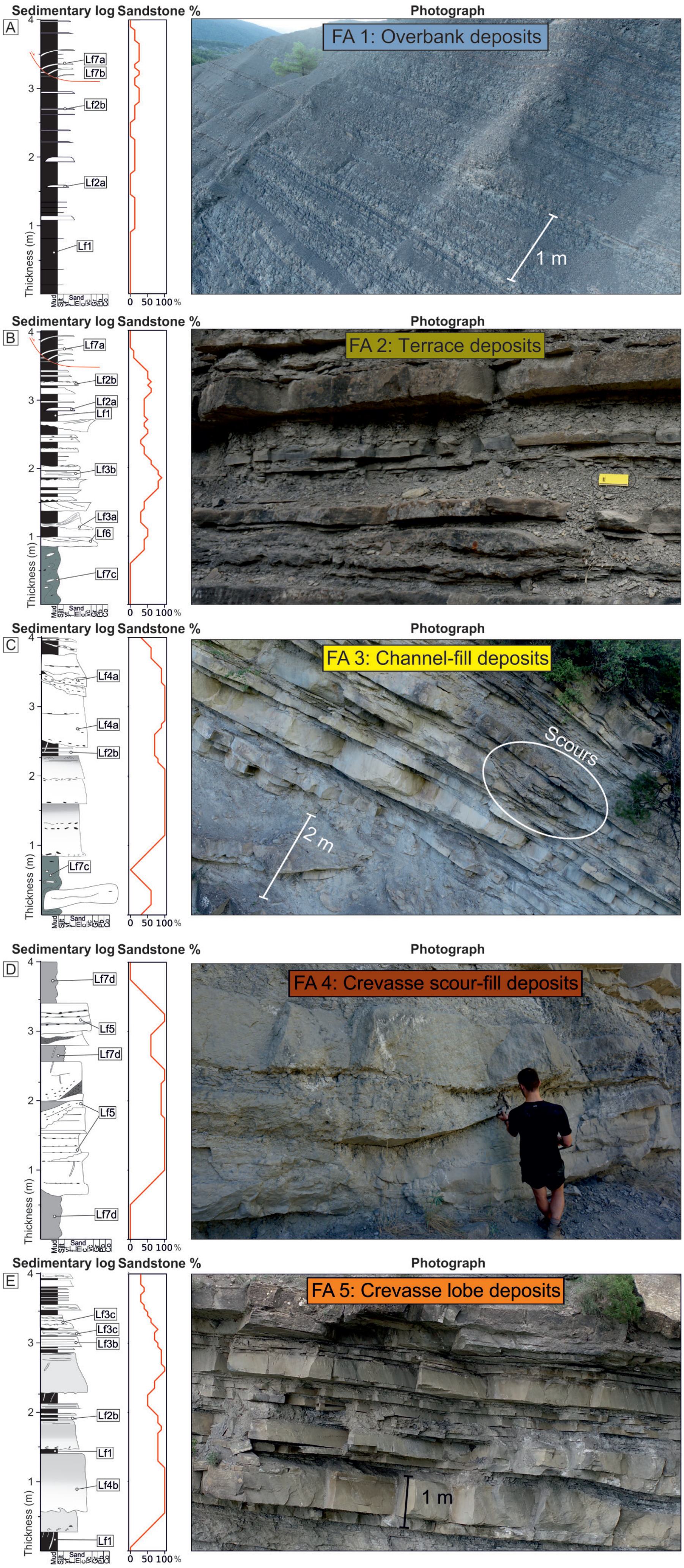

Figure 5 | Representative sedimentary log, sandstone proportion and photograph of the stratal packages representing facies associations (A) FA1: Overbank deposits, (B) FA2: Terrace deposits, (C) FA3: Channel-fill deposits, (D) FA4: Crevasse scour-fill deposits and (E) FA5: Crevasse lobes deposit.

(Lf2b and Lf3b; Figures 2B and 2D) or stoss-side preserved climbing ripples (Lf3c; Figure 2E).

Interpretation: The Lf4b lithofacies within this association suggest rapidly deposited medium- to high-density turbidity currents (sensu Lowe, 1982). Silty tops can be related to an abrupt loss in flow capacity (Hiscott, 1994) due to rapid unconfinement as it exits the crevasse channel/ scours. Planar laminations and stoss side preserved climbing ripples indicate continued bedload traction with high aggradation rates (Sorby, 1859, 1908; Allen, 1973; Jobe, 2012). The intense bioturbation is consistent with proximity to channels, suggesting that these high aspect ratio sand-rich packages are frontal or crevasse lobes (e.g., Morris et al., 2014a, b). The mapping of Bayliss and Pickering (2015) shows that these lobes developed at the flanks of the channel belt rather than at its mouth. Furthermore, they overlie the Banastón II channel-fills and terrace deposits, supporting the interpretation that they represent crevasse lobes rather than frontal lobes (e.g., Beaubouef, 2004; De Ruig and Hubbard, 2006; Hubbard et al., 2009; Morris et al., 2014b).

5. Depositional architecture

The five facies associations (FA1-FA5) described above stack to form two major architectural elements: i) channel belts and ii) structurally confined overbank deposits (Figures 6 and 7).

5.1. Channel belt

Both terrace deposits (FA2) and channel-fill deposits (FA3) suggest deposition within a partly confined/channelised environment, referred to as a channel belt. The mapping from Bayliss and Pickering (2015) and the relatively low divergence in palaeocurrent directions (Figure 8) suggest low-sinuosity channels. The basal debrites (Figures 5B and 5C) suggest an association with submarine landslide emplacement. The abundance of debrites within channel-fill and terrace deposits (Figures 6 and 7) and the mapping from Bayliss and Pickering (2015) suggest that channel belts occupied a topographic low within the Aínsa depocentre. Channel-fill deposits (FA3) are thicker-bedded, more amalgamated, and up to 3 times thicker than the terrace deposits (FA2) (15m vs 5 m), suggesting that the terrace surfaces formed in elevated adjacent areas to the channel (Babonneau et al., 2002, 2004, 2010; Hansen et al., 2015, 2017a, 2017b). The nature of the channel-fill and terrace deposits will vary according to the magnitude of flows along the channel thalweg (Babonneau et al., 2004; Dennielou et al., 2006). Low-magnitude flows are likely to be fully confined within the channel thalweg, and only the upper and more dilute parts of the flow will deposit onto the terrace surfaces, producing fine-grained thin beds (Hansen et al., 2015). In contrast, the lower and upper parts of high-magnitude flows will override the channel margin and terraces, with only the basal part of the flow confined to the channel belt (Babonneau et al., 2004; Hansen et al.,

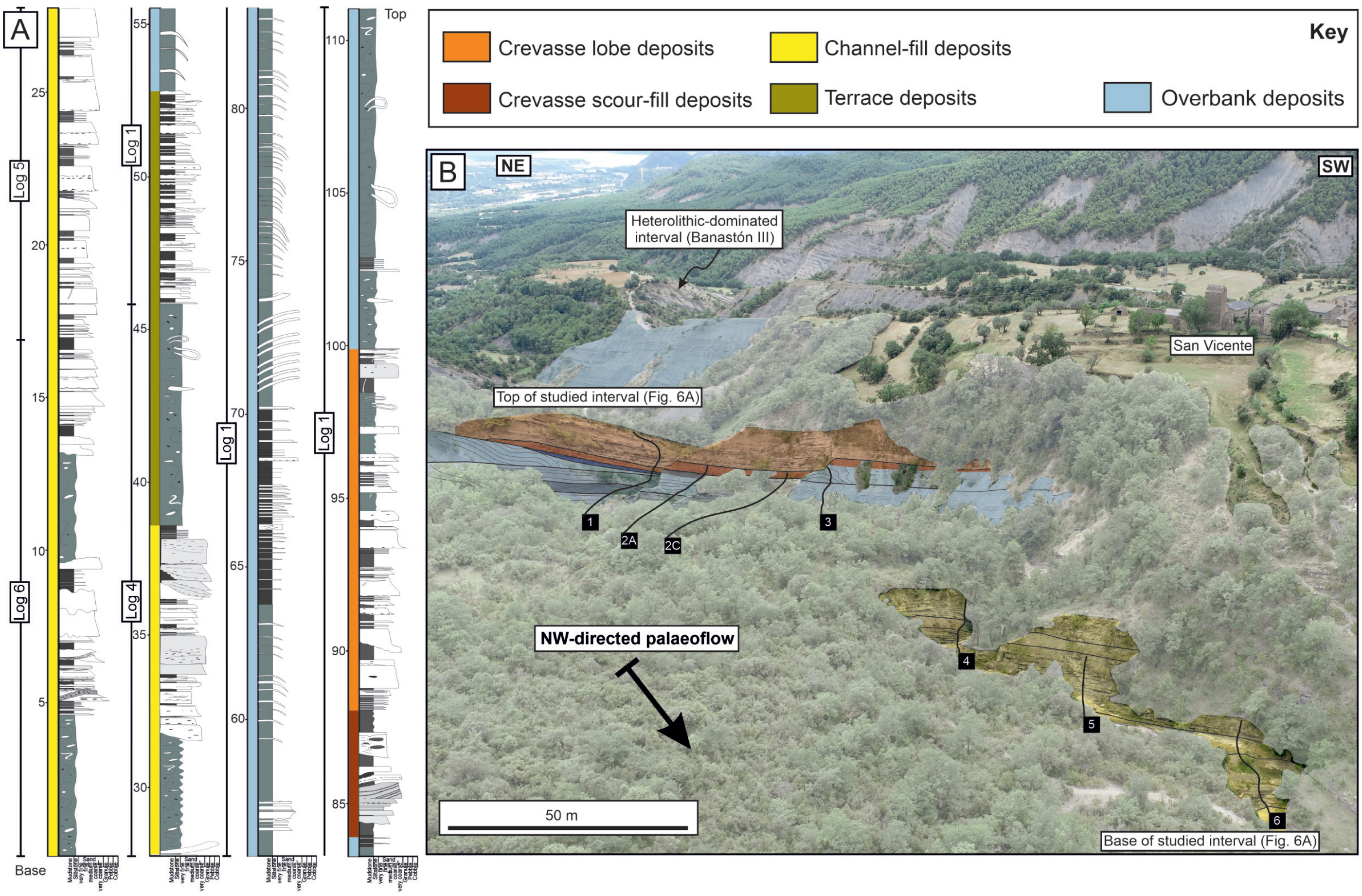

Figure 6 | (A) Composite stratigraphic column of the investigated interval (111 m thick) of the Banastón II member and the different facies associations. (B) Interpreted UAV photographs with the different facies associations and sedimentary logs. Note the village of San Vicente in the top right corner.

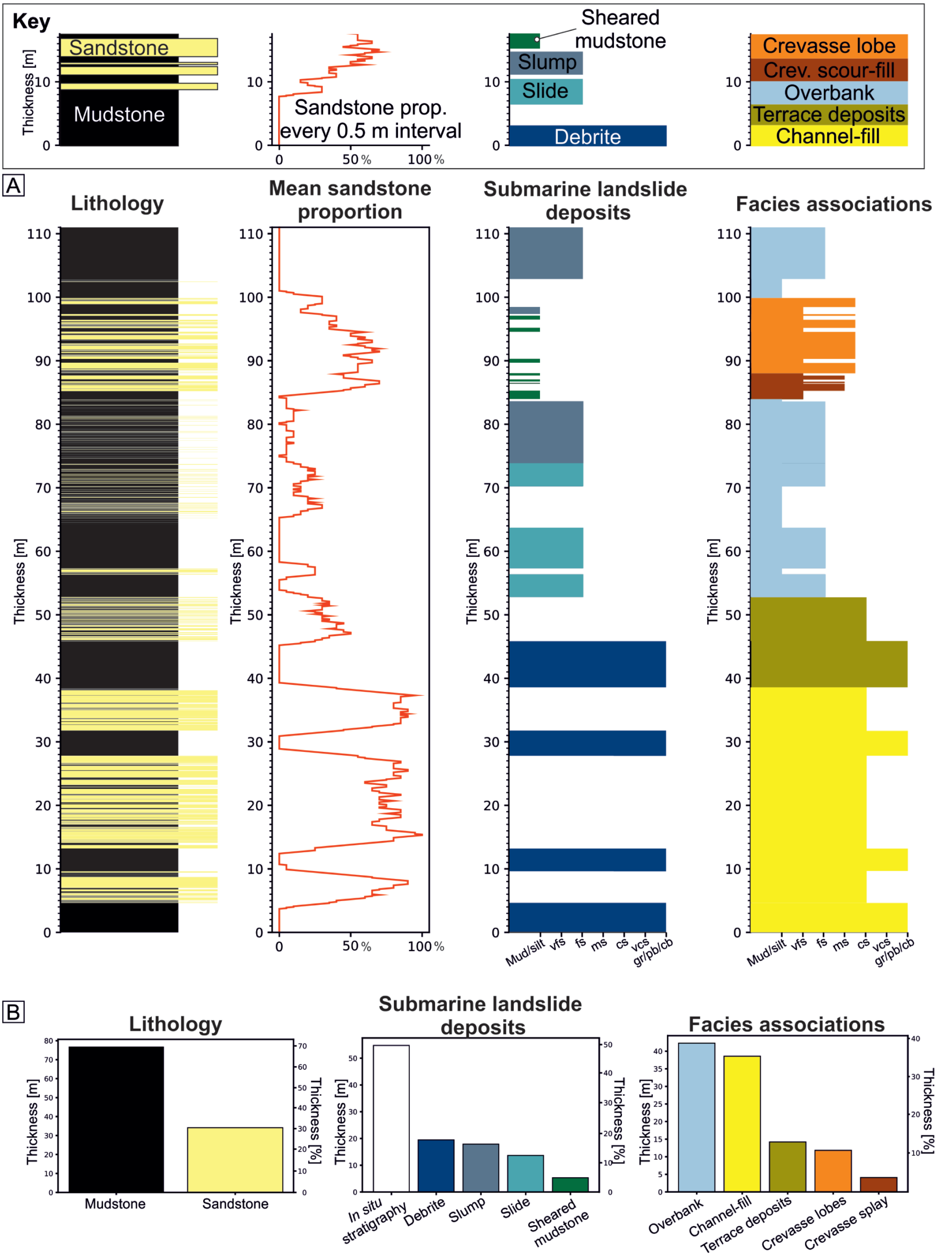

Figure 7 | (A) Logs and (B) histograms showing the lithology, mean sandstone proportion, submarine landslide content and facies associations of the 111 m thick study interval. The mean sandstone proportion is calculated using a moving average with a sample range of 0.5 m. The section is mudstone-dominated, especially on the upper half where the overbank facies association overlies channel-fill and terrace deposits. Note the variation of submarine landslide deposits along the section.

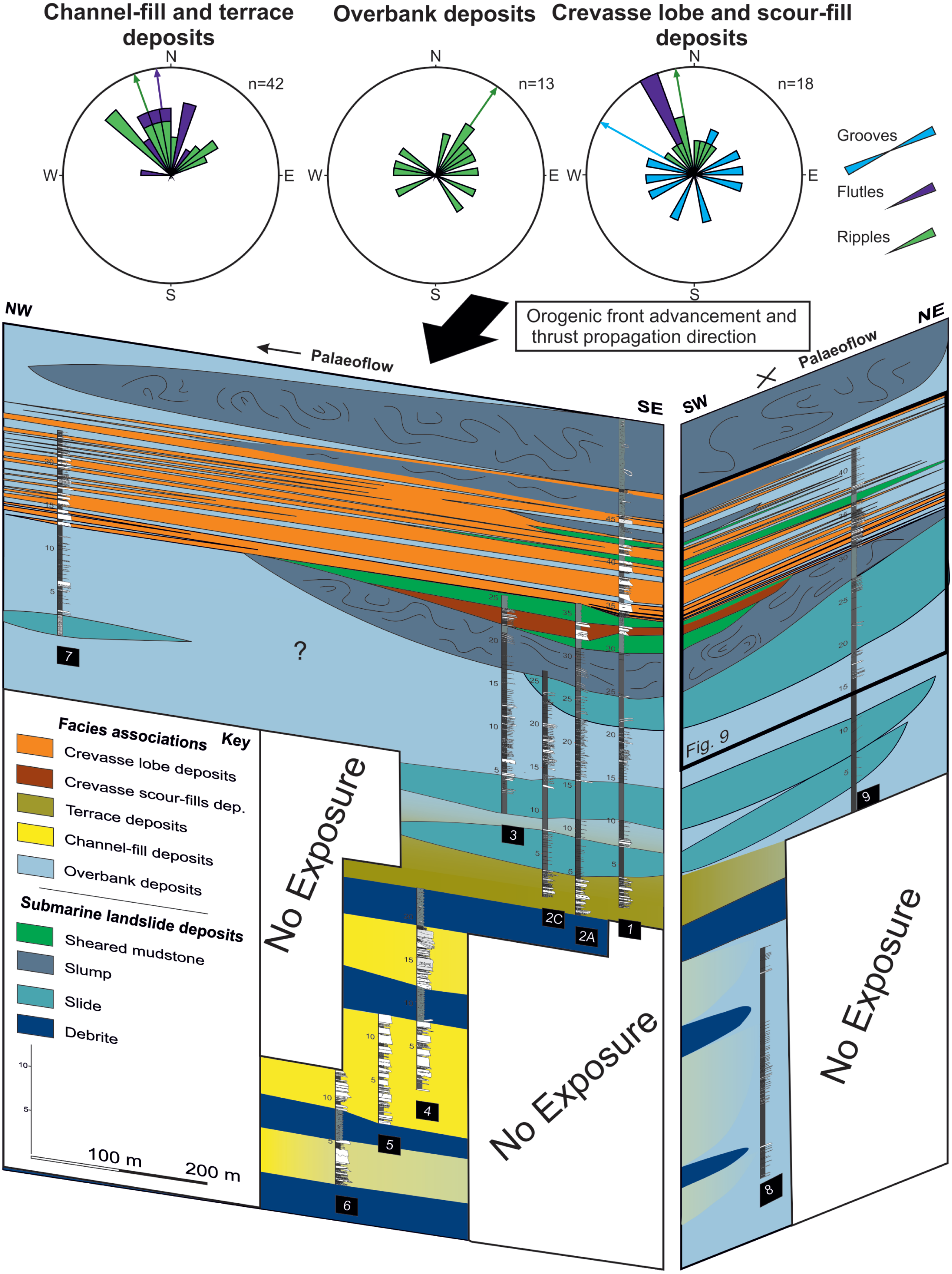

Figure 8 | Correlation panel of the Banastón II member near the San Vicente town. See Figures 1C and 6B for the location of the sedimentary logs. Rose diagrams show palaeocurrent directions. Note that the palaeocurrent directions of the overbank deposits are more northwards directed than in the channel belt and crevasse deposits.

2015, 2017a). High-magnitude flows are likely to result in bypass/erosion within the main channel thalweg, partial bypass and tractional reworking on the terrace, and deposition on the overbank areas if they overspill (Peakall et al., 2000; Kane et al., 2007; Hubbard et al., 2008; Kane and Hodgson, 2011; McArthur et al., 2016; Hansen et al., 2017a). Changes in flow magnitude through time will result in a high degree of variability in bed thicknesses and grain size in the terrace deposits, which are unlikely to be recorded in the channel axis. However, channel-fill deposits (FA3) lack major erosional surfaces (only minor scouring), indicating a depositional phase rather than channel initiation, incision, and bypass. Therefore, the channel-fill deposits recognized in the studied section are likely related to channel abandonment or backfilling (Morris and Normark, 2000; Hodgson et al., 2016).

5.2. Confined overbank

Confined overbank areas consist of three facies associations: overbank (FA1), crevasse scour-fill (FA4), and crevasse lobe (FA5) deposits (Figures 6, 7, and 8), which are interpreted to represent depositional environments outside the channel belt, yet still structurally confined. Overbank deposits are the most abundant facies association, including slumps and slides (Figures 6 and 7). Crevasse scour-fills and crevasse lobes form a 14 metre thick crevasse complex (Figures 9 and 10), interrupting the otherwise monotonous thin-bedded mudstone-dominated overbank deposition. The crevasse complex comprises i) a 4 m thick basal crevasse scour-fill, characterised by poor lateral continuity (FA4), overlain by ii) a 10 m thick thinning-upward laterally continuous package, composed of 1.5 to 5 m thick and at least 1 km long aggradationally stacked crevasse lobes (Figures 8, 9 and 10). Bed thickness and sandstone bed amalgamation decrease upward and laterally in the crevasse complex (Figures 8 and 10). Crevasse lobes are bounded by centimetre-scale mudstone packages (Lf1) and decimetre-scale sheared mudstones (Lf7c). The sheared mudstone packages are only found within the crevasse complex (Figure 7). The lowermost and thickest (up to 5 m) crevasse lobe onlaps onto the slide scar of the underlying slump towards the NE (across strike), with abrupt thinning rates (25 m/km; Figures 6 and 8). However, the slumps are truncated by a SW-dipping surface, interpreted to represent the slide scar of a younger mass failure (Figures 6, 8, and 9). Thinning rates within the crevasse lobe complex are lower towards NW (downdip), where the medium- to thick-bedded sandstones gradually thin (1m/km) into thin-bedded sandstones over 1 km (Figure 8). No bed pinch-out was documented along the downdip transect due to the tabularity of crevasse lobe thin beds (Figure 8). Unlike the lowermost crevasse lobes, the uppermost thin-bedded crevasse lobes do not pass laterally into thick-bedded sandstones, showing a tabular architecture (Figures 6 and 8). The term 'confined overbank' is used here instead of external levees (Kane and Hodgson, 2011) because the tectonic setting of narrow foreland channel systems confined between two opposing slopes (~5-8 km wide syncline) likely resulted in insufficient space to construct wedge-shaped levees. A comparable confinement scale has been documented in the Puchkirchen Formation in the Austrian Molasse Basin (overbank wedges of De Ruig and Hubbard, 2006; Hubbard et al., 2009; Kremer et al., 2018). Tectonically active margins can also promote overbank asymmetry (Kane et al., 2010b; Hansen et al., 2017a; Kneller et al., 2020); therefore, such tectonic control is expected to result in an asymmetry between the northeastern and southwestern overbank deposits of the Banastón II sub-unit. However, the asymmetry of the southwestern overbank area of the Banastón II sub-unit remains unproven, given that it does not crop out and is likely eroded by the channelised flows of the Banaston III.

6. Discussion

6.1. Channel margin collapse and crevasse complex development

During the deposition of the Banastón II sub-unit in the study area, fine-grained sedimentation in the confined overbank areas was interrupted by the deposition of anomalously thick sandstone beds related to developing a crevasse complex. Crevasse complexes result from the breaching of the channel belt (Sawyer et al., 2007, 2014), allowing (parts of) high-density turbidity currents to escape channel-belt confinement (Posamentier and Kolla, 2003; De Ruig and Hubbard, 2006; Hubbard et al., 2009; Armitage et al., 2012; Brunt et al., 2013; Maier et al., 2013; Morris et al., 2014a). The most commonly documented breaching mechanisms are enhanced bank erosion by downstream meander migration (sweep) and/or lateral meander growth (swing) (e.g., Peakall et al., 2000; Abreu et al., 2003; Deptuck et al., 2003) and mechanical weakening by overpressure leading to collapse of channel margins (e.g., Sawyer et al., 2014) or external levees (Ortiz-Karpf et al., 2015). Given the low sinuosity of the Banastón channel, the onlap against a slide scar, and the juxtaposition of the crevasse complex over a slump, channel wall collapse into the channel belt is considered the most plausible mechanism for the initiation of the crevasse complex studied here.

The crevasse scour-fill facies association is interpreted as the most proximal environment of the crevasse complex. Localized acceleration of turbidity currents can produce incisions, promoting further erosion (Eggenhuisen et al., 2011). The juxtaposition of crevasse lobes over crevasse scour-fills might represent a change from bypass to backfilling due to the shape of the slide scar, which is often narrowest at the base and widens upwards. This morphology is likely to promote localised flow constriction (Kneller, 1995), resulting in accumulative (Kneller and Branney, 1995; Kneller and McCaffrey, 1999; Soutter et al., 2021), waxing (Kneller, 1995; Mulder and Alexander, 2001) and partially bypassing turbidity currents (Talling et al., 2012; Stevenson et al., 2015). Substrate excavation

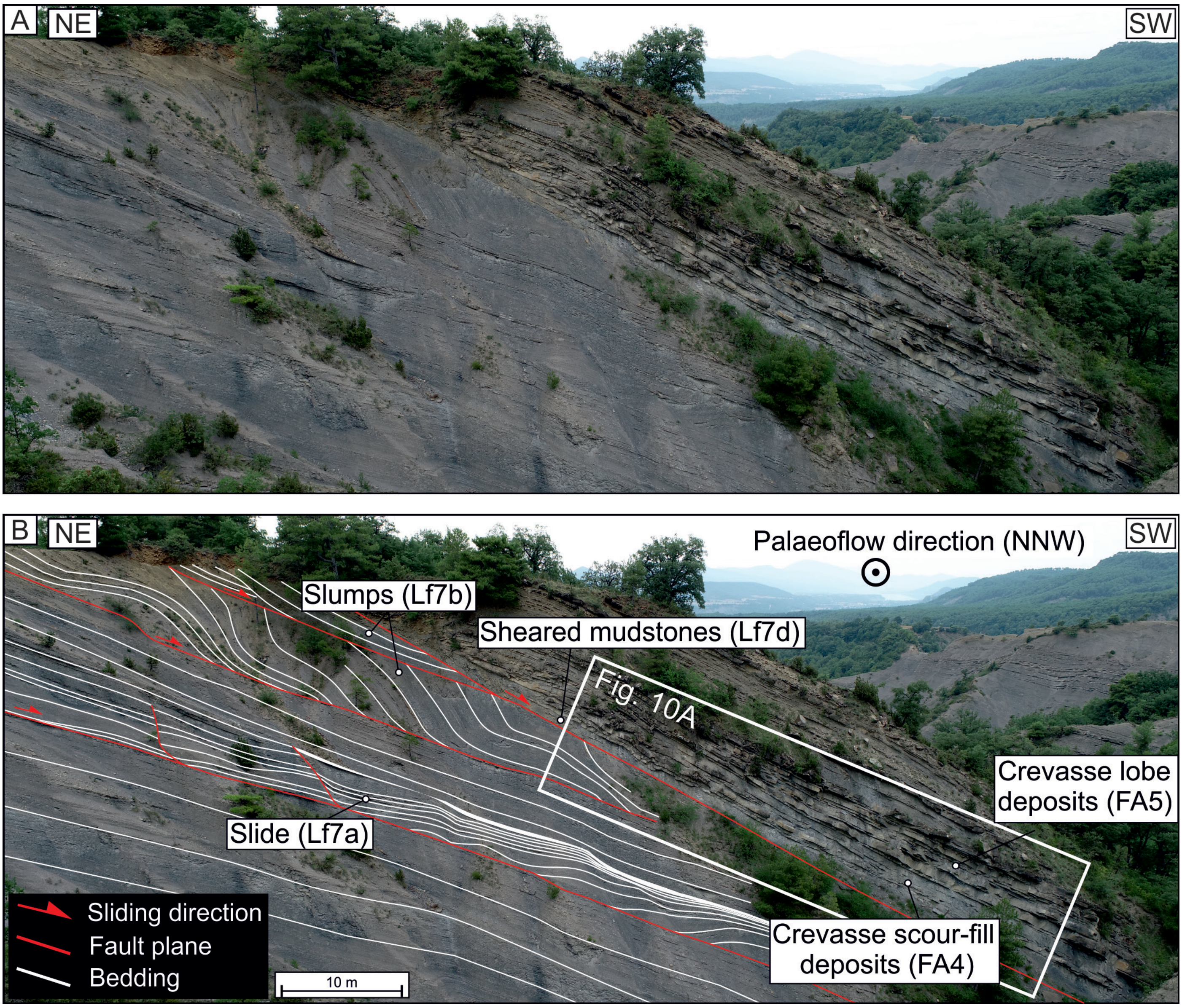

Figure 9 | (A) Unininterpreted and (B) interpreted UAV photographs of the multiple submarine landslides found within the overbank (FA1) and the crevasse scour-fills (FA4) and crevasse lobes deposits (FA5).

can promote local mass failures from slide scar walls, as demonstrated by interfering sand-fill scours (Lf5) and sheared mudstone intervals (Lf7c). This phenomenon has been reported in kilometre-scale submarine landslides, where sidewall fragmentation promotes secondary mass failures and reshapes the original slide scar (Richardson et al., 2011). This effect could increase the aspect ratio (width:height) of the breach, reducing flow constriction and promoting deposition. The upward thinning and fining with increasing tabularity of sandstone beds within the crevasse lobes suggests progressive filling of the accommodation in the confined overbank and/or the abandonment of the adjacent channel through avulsion or reduced sediment supply. Alternatively, it could represent a compensational stacking pattern of crevasse lobes, similar to the crevasse splays documented in fluvial systems (Donselaar et al., 2013; van Toorenenburg et al., 2016; Burns et al., 2019) or in deep-water frontal lobes (Prélat et al., 2009) and that the crevasse scour-fills or crevasse lobes are not necessarily associated with the same crevasse node.

We propose that the nature of the crevasse complex is controlled by the origin of the channel margin collapse scar and subsequent modification and healing, with its stratigraphic evolution reflecting the re-establishment of the overbank area after the breach. Crevasse lobe development has also been observed in the subsurface Puchkirchen Formation in the Austrian Molasse Basin (De Ruig and Hubbard, 2006; Hubbard et al., 2009). However, the crevasse lobes in the Austrian Molasse Basin are not identified on the active margin of the channel system but on the inactive margin. In our study, the abundance of slides and slumps in the studied section (16.1% and 12.2% cumulative thickness, respectively) suggest that they played a key role in creating the conditions to develop crevasse lobes near the active margin. The thickest part of a slide (among other submarine landslides) will likely be found in the lower compressional domain. In contrast, submarine landslides' upper, extensional domain is thinner and might create accommodation toward the slide scar (Figures 10 and 11A; Kremer et al., 2018; Ayckbourne et al., 2023). Breaching by the collapse of the channel margin would leave behind some concave topography susceptible to being exploited as a conduit for subsequent flows (Damuth et al., 1988; Posamentier and Kolla, 2003; Fildani and Normark, 2004; Armitage et al., 2012; Brunt et al., 2013; Maier et al., 2013; Morris et al., 2014a; Ayckbourne et al., 2023). Slide and slump emplacement would also locally reduce the steepness of the active margin and, therefore, the 'valley-confinement.' Thus, flows can escape the channel belt more easily, spreading laterally to deposit sand on the otherwise mudstone-dominated overbank (Figure 11). As the breach is filled, the confinement decreases, and the flows become less erosive, producing a depositional 'backfilling' style. This study, therefore, highlights how local small-scale submarine landslides (in this case <10 m thick) and secondary mass failures can effectively induce crevasse lobe development on active margins and, therefore, provide a means of trapping sand on the slope.

6.2. The impact of submarine landslides on channelised flows and terraces

Submarine landslides are emplaced longitudinally (Bernhardt et al., 2012; Masalimova et al., 2015) and transversely (De Ruig and Hubbard, 2006; Hubbard et al., 2009; Kremer et al., 2018) in peripheral foreland basins. Despite the outcrop limitations and lack of kinematic indicators within the debrites (Bull et al., 2009), the position and composition of submarine landslide deposits within the palaeogeography of the Banastón system suggest that they were emplaced transversely (Bayliss and Pickering, 2015) and probably related to tectonic pulses, given the tectonically active nature of the basin and their abundance. Submarine landslides can disturb the slope equilibrium gradient (Corella et al., 2016; Kremer et al., 2018; Liang et al., 2020; Tek et al., 2020) and induce partial or full blockage of the adjacent conduit (Posamentier and Kolla, 2003; Bernhardt et al., 2012; Corella et al., 2016; Kremer et al., 2018; Tek et al., 2020; Tek et al., 2021; Allen et al., 2022).

Sediment gravity flows passing over debrites can show complex patterns of flow behaviour and resultant deposit character due to the upper surface rugosity of the debrite, which promotes rapid deposition (and associated foundering) and/or erosion and channelisation (Armitage et al., 2009; Fairweather, 2014; Kneller et al., 2016; Valdez et al., 2019; Tek et al., 2020; Martínez-Doñate et al., 2021; Allen et al., 2022). Channelisation can create a positive feedback loop, with enhanced erosion in the channel further increasing confinement (Eggenhuisen et al., 2011; De Leeuw et al., 2016; Hodgson et al., 2016), leading to the development of a conduit bounded laterally by elevated terraces (Hansen et al., 2017b; Tek et al., 2021), as suggested by the fining upward trend recorded in terrace deposits (FA2; Figure 5B). Recent studies based on high-resolution bathymetry and shallow subsurface datasets (Tek et al., 2021) and outcrop studies (Allen et al., 2022) suggest that re-establising previously dammed conduits is complicated by the migration of knickpoints from downstream of the plugging submarine landslide. The high degree of bed amalgamation and lack of metre-scale erosional surfaces in the investigated channel-fill deposits indicate high aggradation rates rather than bypassing sediment gravity flows. We interpret this stratal architecture as indicative of channel backfilling (Pickering et al., 2001) due to damming induced by debrite emplacement or tectonically controlled upstream avulsion due to thrust propagation, as observed in older channel systems within the Aínsa depocentre (Arro system; Millington and Clark, 1995; Tek et al., 2020). Therefore, it is suggested here that the emplacement of submarine landslides within the channel belt impacts channelised flows, and it is the primary mechanism for promoting terrace development in the Banastón II sub-unit.

6.3. Avulsion mechanism(s) in structurally confined channel systems

Long-lived breaching is common on the outer bends of sinuous channels confined by external levees in unconfined settings (Damuth et al., 1988; Posamentier and Kolla, 2003; Fildani and Normark, 2004; Armitage et al., 2012; Brunt et al., 2013; Maier et al., 2013; Morris et al., 2014a) and provides an effective mechanism for the avulsion of the channel system, which might be preceded by the deposition of crevasse lobes (Damuth et al., 1988; Armitage et al., 2012; Brunt et al., 2013; Ortiz-Karpf et al., 2015). However, crevasse lobe development in small, peripheral foreland basin settings is unlikely to lead to avulsion and re-routing of the entire channel belt (Flood et al., 1991) due to low channel sinuosity and structural confinement (Hubbard et al., 2009). The lack of avulsion, related cannibalization of the channel-belt fill, and a confined overbank on the active margin explain why crevasse scour-fills and lobes might be preserved in the Banastón II system. It is unlikely that the emplacement of a few local submarine landslides could drive the avulsion of the entire Banastón II deep-water channel system, given their small size (<10 m thick) compared to the scale of the channel system (98 m thick and 1800 m wide) and the structural confinement (~5-8 km wide syncline; Figure 2). Active tectonism in the foreland basin and related uplift and steepening of the lateral margin likely triggered abundant mass failure events. The progressive uplift and south-westward advancement of the active margin possibly promoted the development of a series of transverse submarine landslides running parallel to the strike of the active margin (Figure 11) that may have enhanced the SW-directed lateral migration of the channel belt (e.g., Posamentier and Kolla, 2003; Deptuck et al., 2007; Kane et al., 2010a; McHargue et al., 2011) as also suggested by Bayliss and Pickering (2015). Even if subsequent channelised sediment gravity flows are not fully ponded after submarine landslide emplacement, they are likely to undergo constriction (Kneller, 1995) and deflection away from the active margin, producing punctuated channel migration (sensu Maier et al., 2012) and breaching. Therefore, we propose that repeated emplacement of submarine landslides, related to the

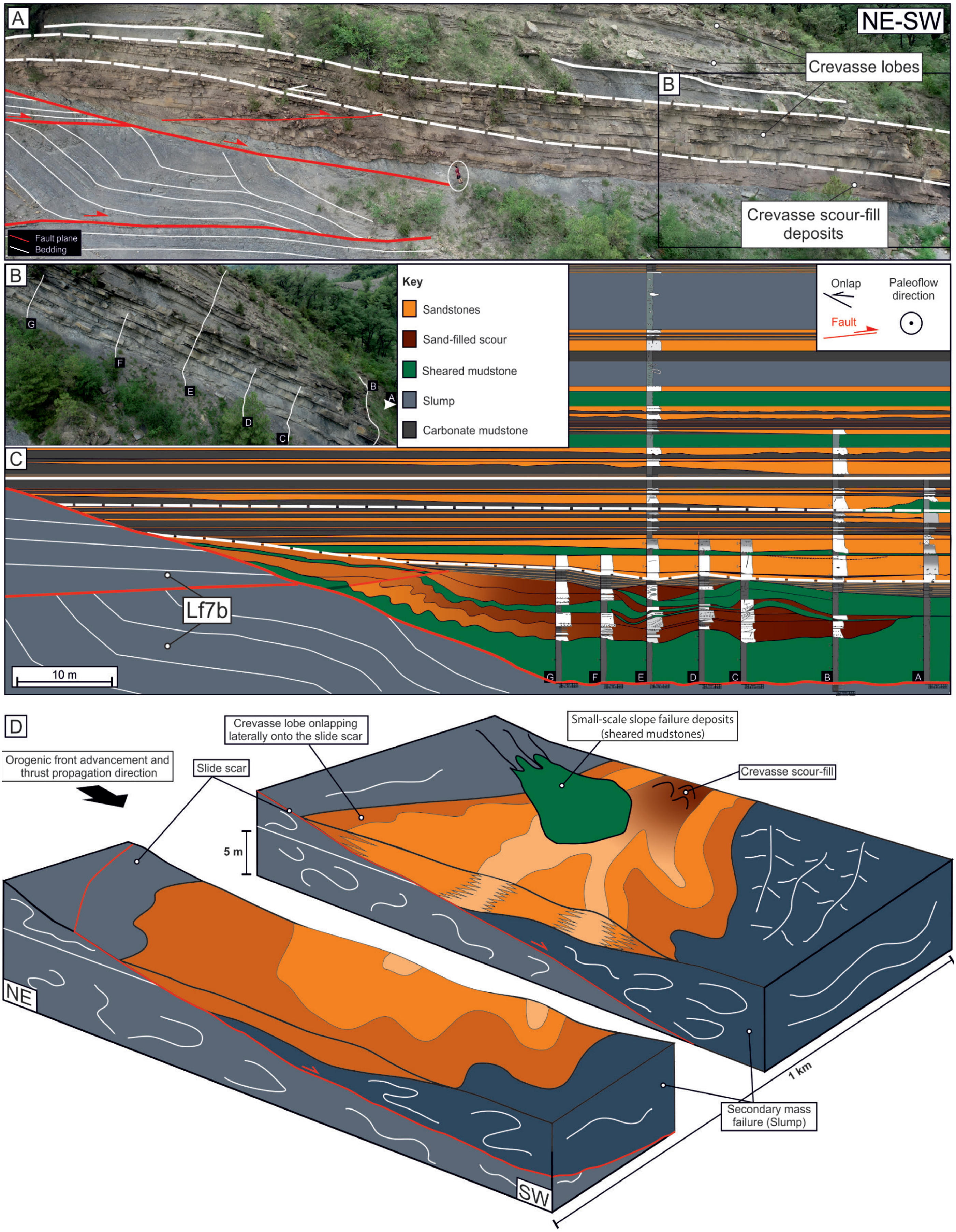

Figure 10 | (A) Interpreted UAV photograph showing a basal slide overlain by the crevasse complex. (B) Location of the sedimentary logs of the crevasse complex. (C) Correlation panel of a crevasse complex showing the juxtaposition of crevasse lobes over the basal crevasse scour-fill deposits. (D) Model illustrating the crevasse lobe juxtaposed over a slump and laterally onlapping the slide scar.

syn-depositional growth of local structures adjacent to channel belts, determined the channel architecture, the sites of crevasse complex deposits, playing a key role in the lateral offset of the Banastón system and storage of sand in the active confining slope.

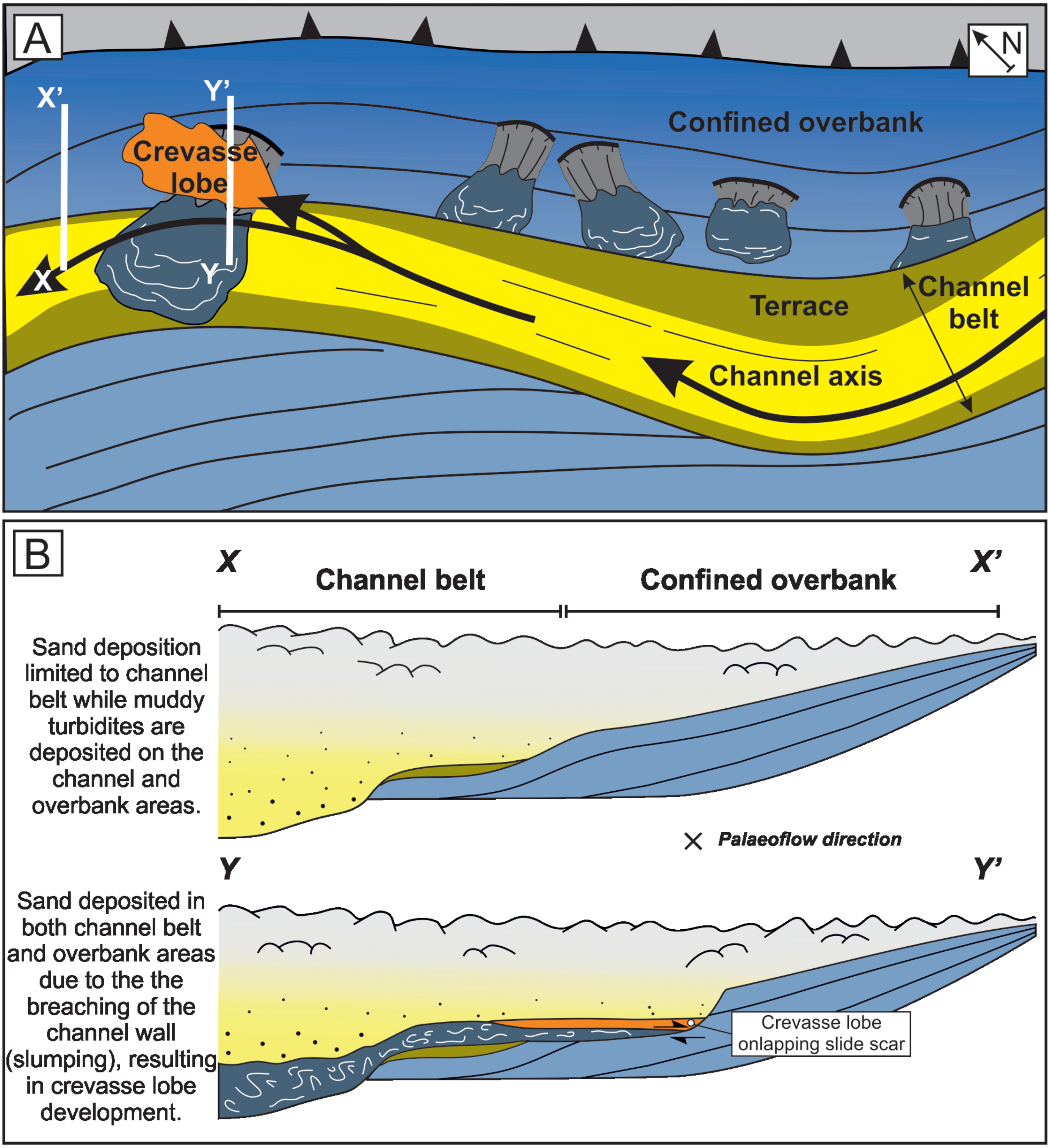

Figure 11 | (A) Evolutionary model illustrating the crevasse lobe deposition on the active margin due to submarine landslide emplacement, deflecting channelised flows towards the slide scar (Modified from De Ruig and Hubbard, 2006) and (B) how the continuous transversely sourced submarine landsliding is a potential mechanism of avulsion of the Banastón II sub-unit.

6.4. Applications of the Banaston system as an analogue

Topographic lows of laterally-confined (slopes dipping 1-10 degrees) deep-water successions are dominated by thick-bedded, tabular, and highly amalgamated deposits (Hurst et al., 1999; Kneller and McCaffrey, 1999; Sinclair, 2000; McCaffrey and Kneller, 2001; Smith and Joseph, 2004; Gardiner, 2006; Bakke et al., 2013; Soutter et al., 2019). Consequently, they are targets for hydrocarbon exploration and production, such as the Oligocene-Miocene Hall and Puchkirchen Formations, which host the main gas reserves in the Austrian Molasse Basin (De Ruig and Hubbard, 2006; Hubbard et al., 2009).

Studying sediment gravity flow deposits and stratal architecture in the subsurface relies on the variable resolution of seismic reflection data and core/well coverage. Therefore, integrating detailed field-based studies such as the one presented here can help bridge the resolution gap, especially at the bed and bedset scale. In exploration, the characterization of communication between the high-quality reservoir sandstones and their updip pinch-out is crucial due to the possibility of fluid migration and associated leakage of hydrocarbons or CO2. Active tectonism and related submarine failures from mudstone-dominated slopes can provide good sealing capacity, especially near the upper slope and canyon areas that are governed by abundant mass failures, as is the case for the Banastón system (Bayliss and Pickering, 2015).

6. Conclusions

The stratigraphic evolution of the Banastón II sub-unit in the San Vicente area records the lateral offset of a submarine channel system, which we relate to the syn-depositional growth of local structures and related mass-wasting events. The active tectonism promoted submarine landslides, which impacted the dynamics of the channel system. The emplacement of debrites within channel belts resulted in channel damming and backfilling. Additionally, modification of the slope gradient caused by the emplacement of debrites was the main mechanism for terrace formation. The emplacement of slides, slumps, and debrites raised the channel base and left concave-up evacuation scars in the confined overbank, which facilitated the formation of breach points exploited by subsequent flows to form crevasse scours and lobes. In contrast to previous studies in similar basin settings, we document that this breaching mechanism occurred towards the active margin instead of the inactive margin. This study highlights that small-scale basin margin failures and their deposits can profoundly influence the dynamics of deep-water channels and their adjacent overbank areas on tectonically confined submarine slopes.

Acknowledgments

This study is a collaboration between The University of Manchester (UK), Universitat Autònoma de Barcelona (Spain) and The University of Leeds (UK). The LOBE 3 consortium project, of which this research forms a part, is supported by sponsorship from Aker BP, BHP, BP, Equinor, HESS, Neptune, Petrobras, PetroChina, Total, Var Energi and Woodside, for which the authors are grateful. We thank Executive Editor Suzanne Bull and reviewers Roberto Tinterri and Rosanna Maniscalco for their reviews and helpful comments that improved the manuscript.

Authors contribution

AMD: Conceptualization, data collection, data analysis, data interpretation, manuscript original draft. ES: Conceptualization, data collection, data interpretation, manuscript review & editing. IK: Conceptualization, data collection, data interpretation, manuscript review & editing. MPM: Conceptualization, data collection, data analysis, data interpretation, manuscript review & editing. DH: Data interpretation, manuscript review & editing. AA: Data analysis, data interpretation, manuscript review & editing. MB: Data interpretation, manuscript review & editing. WT: Data interpretation, manuscript review & editing. SF: Data interpretation, manuscript review & editing

Data availability

The authors confirm that the data supporting all the intepretations are available within the article.

Conflict of interest

The authors declare no conflict of interest in this work.

References

Abreu, V., Sullivan, M., Pirmez, C. & Mohrig, D. (2003) Lateral accretion packages (LAPs): An important reservoir element in deep water sinuous channels. Marine and Petroleum Geology, 20(6), 631–648. https://doi.org/10.1016/j.marpetgeo.2003.08.003

Allen, C., Gomis-Cartesio, L. E., Hodgson, D. M., Peakall, J., & Milana, J. P. (2022). Channel incision into a submarine landslide on a Carboniferous basin margin, San Juan, Argentina: Evidence for the role of knickpoints. The Depositional Record, 8(2), 628-655. https://doi.org/10.1002/dep2.178

Allen, J. R. L. (1971). Instantaneous sediment deposition rates deduced from climbing-ripple cross-lamination. Journal of the Geological Society, 127(6), 553-561.https://doi.org/10.1144/GSL.JGS.1971.127.06.02

Allen, J. R. L. (1973). Phase differences between bed configuration and flow in natural environments, and their geological relevance. Sedimentology, 20(2), 323-329. https://doi.org/10.1111/j.1365-3091.1973.tb02054.x

Allen, J. (1982). Sedimentary structures, their character and physical basis Volume 1. Elsevier. ISBN: 978-0-444-41935-4 ISSN: 0070-4571

Amy, L., Kneller, B., & McCaffrey, W. (2000). Evaluating the Links Between Turbidite Characteristics and Gross System Architecture: Upscaling Insights from the Turbidite Sheet-System of Peïra Cava, SE France", Deep-Water Reservoirs of the World. https://doi.org/10.5724/gcs.00.15.0001

Arbués, P., Mellere, D., Falivene, O., Fernández, O., Muñoz, J.A., Marzo, M. & Gibert, J. M. de (2007). Context and Architecture of the Ainsa-1-Quarry Channel Complex, Spain. AAPG Studies in Geology 56: Atlas of Deep-Water Outcrops, 147, 1-20. https://doi.org/10.1306/12401016St563310

Armitage, D.A., McHargue, T., Fildani, A. and Graham, S.A. (2012). Postavulsion channel evolution: Niger Delta continental slope. Am. Assoc. Pet. Geol. Bull., 96, 823–843. https://doi.org/10.1306/09131110189

Armitage, D. A., McHargue, T., Fildani, A., & Graham, S. A. (2012). Postavulsion channel evolution: Niger Delta continental slope. AAPG bulletin, 96(5), 823-843. https://doi.org/10.2110/jsr.2009.035

Arnott, R. W. C. (2012). Turbidites, and the case of the missing dunes. Journal of Sedimentary Research, 82(6), 379-384. https://doi.org/10.2110/jsr.2012.29

Arnott, R. W. C., & Al-Mufti, O. (2017). Deep-marine pseudo dune cross-stratification—similar, but completely different. Journal of Sedimentary Research, 87(3), 312-323. https://doi.org/10.2110/jsr.2017.21

Ayckbourne, A. J., Jerrett, R. M., Poyatos-Moré, M., Watkinson, M. P., Kane, I. A., & Taylor, K. G. (2023). The influence of creeping slope failure on turbidity current behaviour. Sedimentology, 70(2), 335-361. https://doi.org/10.1111/sed.13049.

Baas, J. H., Best, J. L., & Peakall, J. (2011). Depositional processes, bedform development and hybrid bed formation in rapidly decelerated cohesive (mud–sand) sediment flows. Sedimentology, 58(7), 1953-1987. https://doi.org/10.1111/j.1365-3091.2011.01247.x

Baas, J. H., Best, J. L., & Peakall, J. (2016). Comparing the transitional behaviour of kaolinite and bentonite suspension flows. Earth surface processes and landforms, 41(13), 1911-1921. https://doi.org/10.1002/esp.3959

Baas, J. H., Best, J. L., Peakall, J., & Wang, M. (2009). A phase diagram for turbulent, transitional, and laminar clay suspension flows. Journal of Sedimentary Research, 79(4), 162-183. https://doi.org/10.2110/jsr.2009.025

Babonneau, N., Savoye, B., Cremer, M., & Bez, M. (2010). Sedimentary architecture in meanders of a submarine channel: detailed study of the present Congo turbidite channel (Zaiango project). Journal of Sedimentary Research, 80(10), 852-866. https://doi.org/10.2110/jsr.2010.078

Babonneau, N., Savoye, B., Cremer, M., & Bez, M. (2004). Multiple terraces within the deep incised Zaire Valley (ZaïAngo Project): are they confined levees? Geological Society, London, Special Publications, 222(1), 91-114. https://doi.org/10.1144/GSL.SP.2004.222.01.06

Babonneau, N., Savoye, B., Cremer, M., & Klein, B. (2002). Morphology and architecture of the present canyon and channel system of the Zaire deep-sea fan. Marine and Petroleum Geology, 19(4), 445-467. https://doi.org/10.1016/S0264-8172(02)00009-0

Bakke, K., Kane, I.A., Martinsen, O.J., Petersen, S.A., Johansen, T.A., Hustoft, S., Jacobsen, F.H. & Groth, A. (2013). Seismic modeling in the analysis of deep-water sandstone termination styles. AAPG bulletin, 97(9), 1395-1419. https://doi.org/10.1306/03041312069

Barnolas, A., & Gil-Peña, I. (2001). Ejemplos de relleno sedimentario multiepisódico en una cuenca de antepaís fragmentada: La Cuenca Surpirenaica. Boletín Geológico y Minero, 112(3), 17-38. ISSN: 0366-0176

Bayliss, N., & Pickering, K. T. (2015). Transition from deep-marine lower-slope erosional channels to proximal basin-floor stacked channel–levée–overbank deposits, and syn-sedimentary growth structures, Middle Eocene Banastón System, Ainsa Basin, Spanish Pyrenees. Earth-Science Reviews, 144, 23-46. https://doi.org/10.1016/j.earscirev.2014.11.015

Beaubouef, R. T. (2004). Deep-water leveed-channel complexes of the Cerro Toro Formation, Upper Cretaceous, southern Chile. AAPG bulletin, 88(11), 1471-1500. https://doi.org/10.1306/06210403130

Beaubouef, R. T., & Friedmann, S. J. (2000). High resolution seismic/sequence stratigraphic framework for the evolution of Pleistocene intra slope basins, western Gulf of Mexico: depositional models and reservoir analogs. https://doi.org/10.5724/gcs.00.15.0040

Bell, D., Kane, I. A., Pontén, A. S., Flint, S. S., Hodgson, D. M., & Barrett, B. J. (2018). Spatial variability in depositional reservoir quality of deep-water channel-fill and lobe deposits. Marine and Petroleum Geology, 98, 97-115. https://doi.org/10.1016/j.marpetgeo.2018.07.023

Bernhardt, A., Stright, L., & Lowe, D. R. (2012). Channelized debris-flow deposits and their impact on turbidity currents: The Puchkirchen axial channel belt in the Austrian Molasse Basin. Sedimentology, 59(7), 2042-2070. https://doi.org/10.1111/j.1365-3091.2012.01334.x

Boulesteix, K., Poyatos-Moré, M., Flint, S. S., Hodgson, D. M., Taylor, K. T., & Brunt, R. L. (2022). Sedimentologic and stratigraphic criteria to distinguish between basin-floor and slope mudstones: Implications for the delivery of mud to deep-water environments. The Depositional Record, 8(2), 958-988. https://doi.org/10.1002/dep2.191

Boulesteix, K., Poyatos-Moré, M., Flint, S. S., Taylor, K. G., Hodgson, D. M., & Hasiotis, S. T. (2019). Transport and deposition of mud in deep-water environments: Processes and stratigraphic implications. Sedimentology, 66(7), 2894-2925. https://doi.org/10.1111/sed.12614

Boulesteix, K., Poyatos-Moré, M., Hodgson, D. M., Flint, S. S., & Taylor, K. G. (2020). Fringe or background: Characterizing deep-water mudstones beyond the basin-floor fan sandstone pinchout. Journal of Sedimentary Research, 90(12), 1678-1705. https://doi.org/10.2110/jsr.2020.048

Brunt, R. L., Hodgson, D. M., Flint, S. S., Pringle, J. K., Di Celma, C., Prélat, A., & Grecula, M. (2013). Confined to unconfined: anatomy of a base of slope succession, Karoo Basin, South Africa. Marine and Petroleum Geology, 41, 206-221. https://doi.org/10.1016/j.marpetgeo.2012.02.007

Buffington, E. C. (1952). Submarine" Natural Levees". The Journal of Geology, 60(5), 473-479. https://doi.org/10.1086/625999

Bull, S., Cartwright, J., & Huuse, M. (2009). A review of kinematic indicators from mass-transport complexes using 3D seismic data. Marine and Petroleum Geology, 26(7), 1132-1151. https://doi.org/10.1016/j.marpetgeo.2008.09.011

Burbank, D. W., Puigdefàbregas, C. A. I., & Munoz, J. A. (1992). The chronology of the Eocene tectonic and stratigraphic development of the eastern Pyrenean foreland basin, northeast Spain. Geological Society of America Bulletin, 104(9), 1101-1120. https://doi.org/10.1130/0016-7606(1992)104<1101:TCOTET>2.3.CO;2

Burns, C. E., Mountney, N. P., Hodgson, D. M., & Colombera, L. (2019). Stratigraphic architecture and hierarchy of fluvial overbank splay deposits. Journal of the Geological Society, 176(4), 629-649. https://doi.org/10.1144/jgs2019-001

Caja, M. A., Marfil, R., Garcia, D., Remacha, E., Morad, S., Mansurbeg, H., Amorosi, A., Martínez-Calvo, C., & Lahoz-Beltrá, R. (2010). Provenance of siliciclastic and hybrid turbiditic arenites of the Eocene Hecho Group, Spanish Pyrenees: implications for the tectonic evolution of a foreland basin. Basin Research, 22(2), 157-180. https://doi.org/10.1111/j.1365-2117.2009.00405.x

Canals, M., Casamor, J.L., Urgeles, R., Lastras, G., Calafat, A.M., Masson, D.G., Berné, S. & Alonso, B. (2000). The Ebro Continental Margin, Western Mediterranean Sea: Interplay Between Canyon-Channel Systems and Mass Wasting Processes. Deep-Water Reservoirs of the World, 20, 152–174. https://doi.org/10.5724/gcs.00.15.0152

Cantalejo, B., & Pickering, K. T. (2014). Climate forcing of fine-grained deep-marine systems in an active tectonic setting: Middle Eocene, Ainsa Basin, Spanish Pyrenees. Palaeogeography, Palaeoclimatology, Palaeoecology, 410, 351-371. https://doi.org/10.1016/j.palaeo.2014.06.005

Castelltort, S., Honegger, L., Adatte, T., Clark, J.D., Puigdefàbregas, C., Spangenberg, J.E., Dykstra, M.L. & Fildani, A. (2017). Detecting eustatic and tectonic signals with carbon isotopes in deep-marine strata, Eocene Ainsa Basin, Spanish

Pyrenees. Geology, 45(8), 707-710. https://doi.org/10.1130/G39068.1

Chanvry, E., Deschamps, R., Joseph, P., Puigdefàbregas, C., Poyatos-Moré, M., Serra-Kiel, J., Garcia, D. & Teinturier, S. (2018). The influence of intrabasinal tectonics in the stratigraphic evolution of piggyback basin fills: Towards a model from the Tremp-Graus-Ainsa Basin (South-Pyrenean Zone, Spain). Sedimentary Geology, 377, 34-62. https://doi.org/10.1016/j.sedgeo.2018.09.007

Clark, I. R., & Cartwright, J. A. (2011). Key controls on submarine channel development in structurally active settings. Marine and Petroleum Geology, 28(7), 1333-1349. https://doi.org/10.1016/j.marpetgeo.2011.02.001

Clark, J., Puigdefàbregas, C., Castelltort, S., & Fildani, A. (Eds.). (2017). Propagation of Environmental Signals Within Source-to-sink Stratigraphy: Spanish Pyrenees, June 5th-9th, 2017. SEPM (Society for Sedimentary Geology).

Corella, J.P., Loizeau, J.L., le Dantec, N., Hilbe, M., Gerard, J., le Dantec, N., Stark, N., González-Quijano, M. & Girardclos, S. (2016). The role of mass-transport deposits and turbidites in shaping modern lacustrine deepwater channels. Marine and Petroleum Geology, 77, 515-525. https://doi.org/10.1016/j.marpetgeo.2016.07.004

Dakin, N., Pickering, K. T., Mohrig, D., & Bayliss, N. J. (2013). Channel-like features created by erosive submarine debris flows: field evidence from the Middle Eocene Ainsa Basin, Spanish Pyrenees. Marine and Petroleum Geology, 41, 62-71. https://doi.org/10.1016/j.marpetgeo.2012.07.007

Damuth, J. E., Flood, R. D., Kowsmann, R. O., Belderson, R. H., & Gorini, M. A. (1988). Anatomy and growth pattern of Amazon deep-sea fan as revealed by long-range side-scan sonar (GLORIA) and high-resolution seismic studies. AAPG bulletin, 72(8), 885-911. https://doi.org/10.1306/703C9109-1707-11D7-8645000102C1865D

De Leeuw, J., Eggenhuisen, J. T., & Cartigny, M. J. (2016). Morphodynamics of submarine channel inception revealed by new experimental approach. Nature communications, 7(1), 10886. https://doi.org/10.1038/ncomms10886.

De Ruig, M. J., & Hubbard, S. M. (2006). Seismic facies and reservoir characteristics of a deep-marine channel belt in the Molasse foreland basin, Puchkirchen Formation, Austria. AAPG bulletin, 90(5), 735-752. https://doi.org/10.1306/10210505018

Dennielou, B., Huchon, A., Beaudouin, C., & Berné, S. (2006). Vertical grain-size variability within a turbidite levee: Autocyclicity or allocyclicity? A case study from the Rhône neofan, Gulf of Lions, Western Mediterranean. Marine Geology, 234(1-4), 191-213. https://doi.org/10.1016/j.margeo.2006.09.019

Deptuck, M. E., Steffens, G. S., Barton, M., & Pirmez, C. (2003). Architecture and evolution of upper fan channel-belts on the Niger Delta slope and in the Arabian Sea. Marine and Petroleum Geology, 20(6-8), 649-676. https://doi.org/10.1016/j.marpetgeo.2003.01.004

Deptuck, M. E., Sylvester, Z., Pirmez, C., & O'Byrne, C. (2007). Migration–aggradation history and 3-D seismic geomorphology of submarine channels in the Pleistocene Benin-major Canyon, western Niger Delta slope. Marine and Petroleum Geology, 24(6-9), 406-433. https://doi.org/10.1016/j.marpetgeo.2007.01.005

Donselaar, M. E., Gozalo, M. C., & Moyano, S. (2013). Avulsion processes at the terminus of low-gradient semi-arid fluvial systems: lessons from the Río Colorado, Altiplano endorheic basin, Bolivia. Sedimentary Geology, 283, 1-14. https://doi.org/10.1016/j.sedgeo.2012.10.007

Dreyer, T., Corregidor, J., Arbues, P., & Puigdefabregas, C. (1999). Architecture of the tectonically influenced Sobrarbe deltaic complex in the Ainsa Basin, northern Spain. Sedimentary Geology, 127(3-4), 127-169. https://doi.org/10.1016/S0037-0738(99)00056-1

Eggenhuisen, J. T., McCAFFREY, W. D., Haughton, P. D., & Butler, R. W. (2011). Shallow erosion beneath turbidity currents and its impact on the architectural development of turbidite sheet systems. Sedimentology, 58(4), 936-959. https://doi.org/10.1016/S0037-0738(99)00056-1

Fairweather, L. (2014). Mechanisms of supra MTD topography generation and the interaction of turbidity currents with such deposits (Doctoral dissertation, University of Aberdeen). ISNI:0000 0004 5365 2993

Fernández, O., Muñoz, J. A., Arbués, P., & Falivene, O. (2012). 3D structure and evolution of an oblique system of relaying folds: the Ainsa basin (Spanish Pyrenees). Journal of the Geological Society, 169(5), 545-559. https://doi.org/10.1144/0016-76492011-068

Fildani, A., & Normark, W. R. (2004). Late Quaternary evolution of channel and lobe complexes of Monterey Fan. Marine Geology, 206(1-4), 199-223. https://doi.org/10.1016/j.margeo.2004.03.001

Flood, R. D., Manley, P. L., Kowsmann, R. O., Appi, C. J., & Pirmez, C. (1991). Seismic facies and late Quaternary growth of Amazon submarine fan. In Seismic facies and sedimentary processes of submarine fans and turbidite systems (pp. 415-433). New York, NY: Springer New York. https://doi.org/10.1007/978-1-4684-8276-8

Fontana, D., Zuffa, G. G., & Garzanti, E. (1989). The interaction of eustacy and tectonism from provenance studies of the Eocene Hecho Group Turbidite Complex (South-Central Pyrenees, Spain). Basin Research, 2(4), 223-237. https://doi.org/10.1111/j.1365-2117.1989.tb00037.x

Gardiner, A. R. (2006). The variability of turbidite sandbody pinchout and its impact on hydrocarbon recovery in stratigraphically trapped fields. Geological Society, London, Special Publications, 254(1), 267-287. https://doi.org/10.1144/GSL.SP.2006.254.01.1

Gee, M. J. R., & Gawthorpe, R. L. (2006). Submarine channels controlled by salt tectonics: Examples from 3D seismic data offshore Angola. Marine and Petroleum Geology, 23(4), 443-458. https://doi.org/10.1016/j.marpetgeo.2006.01.002

Georgiopoulou, A., & Cartwright, J. A. (2013). A critical test of the concept of submarine equilibrium profile. Marine and Petroleum Geology, 41, 35-47. https://doi.org/10.1016/j.marpetgeo.2012.03.003

Gupta, K. D., & Pickering, K. T. (2008). Petrography and temporal changes in petrofacies of deep-marine Ainsa–Jaca basin sandstone systems, Early and Middle Eocene, Spanish Pyrenees. Sedimentology, 55(4), 1083-1114. https://doi.org/10.1111/j.1365-3091.2007.00937.x

Hampton, M. A., Lee, H. J., & Locat, J. (1996). Submarine landslides. Reviews of geophysics, 34(1), 33-59. https://doi.org/10.1029/95RG03287

Hansen, L., Callow, R., Kane, I., & Kneller, B. (2017a). Differentiating submarine channel-related thin-bedded turbidite facies: Outcrop examples from the Rosario Formation, Mexico. Sedimentary Geology, 358, 19-34. https://doi.org/10.1016/j.sedgeo.2017.06.009

Hansen, L. A., Callow, R. H., Kane, I. A., Gamberi, F., Rovere, M., Cronin, B. T., & Kneller, B. C. (2015). Genesis and character of thin-bedded turbidites associated with submarine channels. Marine and Petroleum Geology, 67, 852-879. https://doi.org/10.1016/j.marpetgeo.2015.06.007

Hansen, L. A. S., Hodgson, D. M., Pontén, A., Thrana, C., & Latre, A. O. (2021). Mixed axial and transverse deep-water systems: The Cretaceous post-rift Lysing Formation, offshore Norway. Basin Research, 33(4), 2229-2251. https://doi.org/10.1111/bre.12555

Hansen, L., Janocko, M., Kane, I., & Kneller, B. (2017b). Submarine channel evolution, terrace development, and preservation of intra-channel thin-bedded turbidites: Mahin and Avon channels, offshore Nigeria. Marine Geology, 383, 146-167. https://doi.org/10.1016/j.margeo.2016.11.011

Heezen, B. C., Ewing, M., & Menzies, R. J. (1955). The influence of submarine turbidity currents on abyssal productivity. Oikos, 6(2), 170-182. https://doi.org/10.2307/3564853

Heiniö, P., & Davies, R. J. (2007). Knickpoint migration in submarine channels in response to fold growth, western Niger Delta. Marine and Petroleum Geology, 24(6-9), 434-449. https://doi.org/10.1016/j.marpetgeo.2006.09.002

Hiscott, R. N. (1994). Loss of capacity, not competence, as the fundamental process governing deposition from turbidity currents. Journal of Sedimentary Research, 64(2a), 209-214. https://doi.org/10.2110/jsr.64.209

Hodgson, D. M., Kane, I. A., Flint, S. S., Brunt, R. L., & Ortiz-Karpf, A. (2016). Time-transgressive confinement on the slope and the progradation of basin-floor fans: Implications for the sequence stratigraphy of deep-water deposits. Journal of Sedimentary Research, 86(1), 73-86. https://doi.org/10.2110/jsr.2016.3

Hofstra, M., Peakall, J., Hodgson, D. M., & Stevenson, C. J. (2018). Architecture and morphodynamics of subcritical sediment waves in an ancient channel–lobe transition zone. Sedimentology, 65(7), 2339-2367. https://doi.org/10.1111/sed.12468

Hubbard, S. M., de Ruig, M. J., & Graham, S. A. (2009). Confined channel-levee complex development in an elongate depo-center: deep-water Tertiary strata of the Austrian Molasse basin. Marine and Petroleum Geology, 26(1), 85-112. https://doi.org/10.1016/j.marpetgeo.2007.11.006

Hübscher, C., Spiess, V., Breitzke, M., & Weber, M. E. (1997). The youngest channel-levee system of the Bengal Fan: results from digital sediment echosounder data. Marine Geology, 141(1-4), 125-145. https://doi.org/10.1016/S0025-3227(97)00066-2

Hurst, A., Verstralen, I., Cronin, B., & Hartley, A. (1999). Sand-rich fairways in deep-water clastic reservoirs: genetic units, capturing uncertainty, and a new approach to reservoir modeling. AAPG bulletin, 83(7), 1096-1118. https://doi.org/10.1306/E4FD2E83-1732-11D7-8645000102C1865D

Jobe, Z. R., Lowe, D. R., & Morris, W. R. (2012). Climbing-ripple successions in turbidite systems: depositional environments, sedimentation rates and accumulation times. Sedimentology, 59(3), 867-898. https://doi.org/10.1111/j.1365-3091.2011.01283.x

Kane, I. A., Catterall, V., McCaffrey, W. D., & Martinsen, O. J. (2010). Submarine channel response to intrabasinal tectonics: The influence of lateral tilt. AAPG bulletin, 94(2), 189-219. https://doi.org/10.1306/08180909059

Kane, I. A., & Clare, M. A. (2019). Dispersion, accumulation, and the ultimate fate of microplastics in deep-marine environments: a review and future directions. Frontiers in earth science, 7, 80. https://doi.org/10.3389/feart.2019.00080

Kane, I. A., & Hodgson, D. M. (2011). Sedimentological criteria to differentiate submarine channel levee subenvironments: exhumed examples from the Rosario Fm.(Upper Cretaceous) of Baja California, Mexico, and the Fort Brown Fm.(Permian), Karoo basin, S. Africa. Marine and Petroleum Geology, 28(3), 807-823. https://doi.org/10.1016/j.marpetgeo.2010.05.009

Kane, I. A., Kneller, B. C., Dykstra, M., Kassem, A., & McCaffrey, W. D. (2007). Anatomy of a submarine channel–levee: an example from Upper Cretaceous slope sediments, Rosario Formation, Baja California, Mexico. Marine and Petroleum Geology, 24(6-9), 540-563. https://doi.org/10.1016/j.marpetgeo.2007.01.003

Kane, I. A., McCaffrey, W. D., & Martinsen, O. J. (2009). Allogenic vs. autogenic controls on megaflute formation. Journal of Sedimentary Research, 79(9), 643-651. https://doi.org/10.2110/jsr.2009.072

Kane, I. A., McCaffrey, W. D., Peakall, J., & Kneller, B. C. (2010). Submarine channel levee shape and sediment waves from physical experiments. Sedimentary Geology, 223(1-2), 75-85. https://doi.org/10.1016/j.sedgeo.2009.11.001

Kane, I.A., McGee, T.D., Jobe, Z.R. (2012). Halokinetic effects on slope equilibrium profiles: Submarine channel evolution and implications for facies architecture in Magnolia field, Gulf of Mexico. Salt Tectonics, Sediments and Prospectivity. Geological Society of London, 363, 289-302. https://doi.org/10.1144/SP363.13

Keevil, G. M., Peakall, J., Best, J. L., & Amos, K. J. (2006). Flow structure in sinuous submarine channels: Velocity and turbulence structure of an experimental submarine channel. Marine Geology, 229(3-4), 241-257. https://doi.org/10.1016/j.margeo.2006.03.010

Kneller, B. (1995). Beyond the turbidite paradigm: physical models for deposition of turbidites and their implications for reservoir prediction. Geological Society, London, Special Publications, 94(1), 31-49. https://doi.org/10.1144/GSL.SP.1995.094.01.04

Kneller, B., Bozetti, G., Callow, R., Dykstra, M., Hansen, L., Kane, I., Li, P., McArthur, A., Catharina, A.S., Dos Santos, T. & Thompson, P. (2020). Architecture, process, and environmental diversity in a late Cretaceous slope channel system. Journal of Sedimentary Research, 90(1), 1-26. https://doi.org/10.2110/jsr.2020.1

Kneller, B., Edwards, D., McCaffrey, W., & Moore, R. (1991). Oblique reflection of turbidity currents. Geology, 19(3), 250-252. https://doi.org/10.1130/0091-7613(1991)019<0250:OROTC>2.3.CO;2

Kneller, B. C., & Branney, M. J. (1995). Sustained high-density turbidity currents and the deposition of thick massive sands. Sedimentology, 42(4), 607-616. https://doi.org/10.1111/j.1365-3091.1995.tb00395.x

Kneller, B., Dykstra, M., Fairweather, L., & Milana, J. P. (2016). Mass-transport and slope accommodation: Implications for turbidite sandstone reservoirs. AAPG bulletin, 100(2), 213-235. https://doi.org/10.1306/09011514210

Kneller, B. C., & McCaffrey, W. D. (2003). The interpretation of vertical sequences in turbidite beds: the influence of longitudinal flow structure. Journal of Sedimentary Research, 73(5), 706-713. https://doi.org/10.1306/031103730706

Kneller, B., & McCaffrey, W. (1999). Depositional effects of flow nonuniformity and stratification within turbidity currents approaching a bounding slope; deflection, reflection, and facies variation. Journal of Sedimentary Research, 69(5), 980-991. https://doi.org/10.2110/jsr.69.980

Kremer, C. H., McHargue, T., Scheucher, L., & Graham, S. A. (2018). Transversely-sourced mass-transport deposits and stratigraphic evolution of a foreland submarine channel system: Deep-water tertiary strata of the Austrian Molasse Basin. Marine and Petroleum Geology, 92, 1-19. https://doi.org/10.1016/j.marpetgeo.2018.01.035

Läuchli, C., Garcés, M., Beamud, E., Valero, L., Honegger, L., Adatte, T., Spangenberg, J.E., Clark, J., Puigdefàbregas, C., Fildani, A., de Kaenel, E., Hunger, T., Nowak, A. & Castelltort, S. (2021). Magnetostratigraphy and stable isotope stratigraphy of the middle-Eocene succession of the Ainsa basin (Spain): New age constraints and implications for sediment delivery to the deep waters. Marine and Petroleum Geology, 132, 105182. https://doi.org /10.1016/j.marpetgeo.2021.105182

Liang, C., Xie, X., He, Y., Chen, H., Yu, X., Zhang, W., Mi, H., Lu, B., Tian, D., Zhang, H., Li, M. & Zhou, Z. (2020). Multiple sediment sources and topographic changes controlled the depositional architecture of a palaeoslope-parallel canyon in the Qiongdongnan Basin, South China Sea. Marine and Petroleum Geology, 113, 104161. https://doi.org/10.1016/j.marpetgeo.2019.104161

Lowe, D. R. (1982). Sediment gravity flows; II, Depositional models with special reference to the deposits of high-density turbidity currents. Journal of sedimentary research, 52(1), 279-297. https://doi.org/10.1306/212F7F31-2B24-11D7-8648000102C1865D

Maier, K.L., Fildani, A., McHargue, T.R., Paull, C.K., Graham, S.A., and Caress, D.W. (2012). Punctuated deep-water channel migration: high-resolution subsurface data from the Lucia Chica channel system, offshore California, U.S.A. Journal of Sedimentary Research, 82, 1–8. https://doi.org/10.2110/jsr.2013.6

Maier, K. L., Fildani, A., Paull, C. K., McHargue, T. R., Graham, S. A., & Caress, D. W. (2013). Deep-sea channel evolution and stratigraphic architecture from inception to abandonment from high-resolution autonomous underwater vehicle surveys offshore central California. Sedimentology, 60(4), 935-960. https://doi.org/10.1111/j.1365-3091.2012.01371.x

Martínez-Doñate, A., Privat, A.M.L.J., Hodgson, D.M., Jackson, C.A.L., Kane, I.A., Spychala, Y.T., Duller, R.A., Stevenson, C., Keavney, E., Schwarz, E. & Flint, S.S. (2021). Substrate entrainment, depositional relief, and sediment capture: Impact of a submarine landslide on flow process and sediment supply. Frontiers in Earth Science, 9, 757617. https://doi.org/10.3389/feart.2021.757617

Masalimova, L. U., Lowe, D. R., Mchargue, T., & Derksen, R. (2015). Interplay between an axial channel belt, slope gullies and overbank deposition in the Puchkirchen Formation in the Molasse Basin, Austria. Sedimentology, 62(6), 1717-1748. https://doi.org/10.1111/sed.12201

McArthur, A. D., Hartley, A. J., Archer, S. G., Jolley, D. W., & Lawrence, H. M. (2016). Spatiotemporal relationships of deep-marine, axial, and transverse depositional systems from the synrift Upper Jurassic of the central North Sea. AAPG Bulletin, 100(9), 1469-1500. https://doi.org/10.1306/04041615125

McCaffrey, W., & Kneller, B. (2001). Process controls on the development of stratigraphic trap potential on the margins of confined turbidite systems and aids to reservoir evaluation. AAPG bulletin, 85(6), 971-988. https://doi.org/10.1306/8626CA41-173B-11D7-8645000102C1865D

McHargue, T., Pyrcz, M.J., Sullivan, M.D., Clark, J.D., Fildani, A., Romans, B.W., Covault, J.A., Levy, M., Posamentier, H.W. & Drinkwater, N.J. (2011). Architecture of turbidite channel systems on the continental slope: patterns and predictions. Marine and petroleum geology, 28(3), 728-743. https://doi.org/10.1016/j.marpetgeo.2010.07.008

Menard Jr, H. W. (1955). Deep-sea channels, topography, and sedimentation. AAPG Bulletin, 39(2), 236-255. https://doi.org/10.1306/5CEAE136-16BB-11D7-8645000102C1865D

Millington, J. J., & Clark, J. D. (1995). The Charo/Arro canyon-mouth sheet system, south-central Pyrenees, Spain; a structurally influenced zone of sediment dispersal. Journal of Sedimentary Research, 65(4b), 443-454. https://doi.org/10.1306/D426827F-2B26-11D7-8648000102C1865D

Morris, E. A., Hodgson, D. M., Brunt, R. L., & Flint, S. S. (2014a). Origin, evolution and anatomy of silt-prone submarine external levées. Sedimentology, 61(6), 1734-1763. https://doi.org/10.1111/sed.12114

Morris, E. A., Hodgson, D. M., Flint, S. S., Brunt, R. L., Butterworth, P. J., & Verhaeghe, J. (2014b). Sedimentology, stratigraphic architecture, and depositional context of submarine frontal-lobe complexes. Journal of Sedimentary Research, 84(9), 763-780. https://doi.org/10.2110/jsr.2014.61

Moscardelli, L., & Wood, L. (2008). New classification system for mass transport complexes in offshore Trinidad. Basin research, 20(1), 73-98. https://doi.org/10.1111/j.1365-2117.2007.00340.x

Mulder, T., & Alexander, J. (2001). The physical character of subaqueous sedimentary density flows and their deposits. Sedimentology, 48(2), 269-299. https://doi.org/10.1046/j.1365-3091.2001.00360.x

Muñoz, J. A. (1992). Evolution of a continental collision belt: ECORS-Pyrenees crustal balanced cross-section. In Thrust tectonics (pp. 235-246). Dordrecht: Springer Netherlands. https://doi.org/10.1007/978-94-011-3066-0_21

Muñoz, J.A., 2002. The Pyrenees. In: Gibbons, W., Moreno, T. (eds.). The Geology of Spain. The Geological Society of London, 370-385. https://doi.org/10.1144/GOSPP

Muñoz, J. A., Beamud, E., Fernández, O., Arbués, P., Dinarès-Turell, J., & Poblet, J. (2013). The Ainsa Fold and thrust oblique zone of the central Pyrenees: Kinematics of a curved contractional system from paleomagnetic and structural data. Tectonics, 32(5), 1142-1175. https://doi.org/10.1002/tect.20070.

Mutti, E. (1991). Distinctive thin-bedded turbidite facies and related depositional environments in the Eocene Hecho Group (South-central Pyrenees, Spain). Deep-Water Turbidite Systems, 181-205. https://doi.org/10.1002/9781444304473.ch14

Mutti, E. (1992). Turbidite Sandstones. San Donato Milanese, Italy: Agip-Istituto di Geologia, Università di Parma. 275.

Mutti, E., Luterbacher, H.P., Ferrer, J. and Rosell, J. (1972). Schema stratigrafico e lineamenti di facies del Paleogene marino della zona centrale sudpirenaica tra temp (Catalogna) e Pamplona (Navarra). Societa Geologica Italiana, 11, 391–416. http://pascal-francis.inist.fr/vibad/index.php?action=getRecordDetail&idt=PASCALGEODEBRGM732243900

Mutti, E., & Normark, W. R. (1991). An integrated approach to the study of turbidite systems. In Seismic facies and sedimentary processes of submarine fans and turbidite systems (pp. 75-106). New York, NY: Springer New York. https://doi.org/10.1007/978-1-4684-8276-8_4

Nardin, T. R., Hein, F. J., Gorsline, D. S., & Edwards, B. D. (1979). A review of mass movement processes, sediment and acoustic characteristics, and contrasts in slope and base-of-slope systems versus canyon-fan-basin floor systems. https://doi.org/10.2110/pec.79.27.0061

Nijman, W. (1998). Cyclicity and basin axis shift in a piggyback basin: towards modelling of the Eocene Tremp-Ager Basin, South Pyrenees, Spain. Geological Society, London, Special Publications, 134(1), 135-162. https://doi.org/10.1144/GSL.SP.1998.134.01.07

Normark, W. R. (1970). Growth patterns of deep-sea fans. AAPG bulletin, 54(11), 2170-2195. https://doi.org/10.1306/5D25CC79-16C1-11D7-8645000102C1865D

Nwoko, J., Kane, I., & Huuse, M. (2020). Mass transport deposit (MTD) relief as a control on post-MTD sedimentation: Insights from the Taranaki Basin, offshore New Zealand. Marine and Petroleum Geology, 120, 104489. https://doi.org/10.1016/j.marpetgeo.2020.104489.

Ortiz-Karpf, A., Hodgson, D. M., & McCaffrey, W. D. (2015). The role of mass-transport complexes in controlling channel avulsion and the subsequent sediment dispersal patterns on an active margin: the Magdalena Fan, offshore Colombia. Marine and Petroleum Geology, 64, 58-75. https://doi.org/10.1016/j.marpetgeo.2015.01.005

Payros, A., Tosquella, J., Bernaola, G., Dinarès-Turell, J., Orue-Etxebarria, X., & Pujalte, V. (2009). Filling the North European Early/Middle Eocene (Ypresian/Lutetian) boundary gap: Insights from the Pyrenean continental to deep-marine record. Palaeogeography, Palaeoclimatology, Palaeoecology, 280(3-4), 313-332. https://doi.org/10.1016/j.palaeo.2009.06.018

Peakall, J., McCaffrey, B., & Kneller, B. (2000). A process model for the evolution, morphology, and architecture of sinuous submarine channels. Journal of Sedimentary Research, 70(3), 434-448. https://doi.org/10.1306/2DC4091C-0E47-11D7-8643000102C1865D

Pemberton, E. A., Hubbard, S. M., Fildani, A., Romans, B., & Stright, L. (2016). The stratigraphic expression of decreasing confinement along a deep-water sediment routing system: Outcrop example from southern Chile. Geosphere, 12(1), 114-134. https://doi.org/10.1130/GES01233.1

Pickering, K. T., & Bayliss, N. J. (2009). Deconvolving tectono-climatic signals in deep-marine siliciclastics, Eocene Ainsa basin, Spanish Pyrenees: Seesaw tectonics versus eustasy. Geology, 37(3), 203-206. https://doi.org/10.1130/G25261A.1

Pickering, K. T., & Corregidor, J. (2005). Mass-transport complexes (MTCs) and tectonic control on basin-floor submarine fans, middle Eocene, south Spanish Pyrenees. Journal of Sedimentary Research, 75(5), 761-783. https://doi.org/10.2110/jsr.2005.062

Pickering, K. T., & Hiscott, R. N. (1991). Contained (reflected) turbidity currents from the Middle Ordovician Cloridorme Formation, Quebec, Canada: an alternative to the antidune hypothesis. Deep-Water Turbidite Systems, 89-110. https://doi.org/10.1002/9781444304473.ch6

Pickering, K. T., Hodgson, D. M., Platzman, E., Clark, J. D., & Stephens, C. (2001). A new type of bedform produced by backfilling processes in a submarine channel, late Miocene, Tabernas-Sorbas basin, SE Spain. Journal of Sedimentary Research, 71(5), 692-704. https://doi.org/10.1306/2DC40960-0E47-11D7-8643000102C1865D

Pinter, P. R., Butler, R. W., Hartley, A. J., Maniscalco, R., Baldassini, N., & Di Stefano, A. (2018). Tracking sand-fairways through a deformed turbidite system: The numidian (Miocene) of Central Sicily, Italy. Basin Research, 30(3), 480-501. https://doi.org/10.1111/bre.12261

Piper, D. J., & Normark, W. R. (1983). Turbidite depositional patterns and flow characteristics, Navy submarine fan, California Borderland. Sedimentology, 30(5), 681-694. https://doi.org/10.1111/j.1365-3091.1983.tb00702.x

Piper, D. J., & Normark, W. R. (2001). Sandy fans-from Amazon to Hueneme and beyond. AAPG bulletin, 85(8), 1407-1438. https://doi.org/10.1306/8626CACD-173B-11D7-8645000102C1865D

Poblet, J., Muñoz, J. A., Travé, A., & Serra-Kiel, J. (1998). Quantifying the kinematics of detachment folds using three-dimensional geometry: Application to the Mediano anticline (Pyrenees, Spain). Geological Society of America Bulletin, 110(1), 111-125. https://doi.org/10.1130/0016-7606(1998)110<0111:QTKODF>2.3.CO;2

Pohl, F., Eggenhuisen, J. T., Cartigny, M. J. B., Tilston, M. C., de Leeuw, J., & Hermidas, N. (2020). The influence of a slope break on turbidite deposits: an experimental investigation. Marine Geology, 424, 106160. https://doi.org/10.1016/j.margeo.2020.106160

Posamentier, H. W., & Kolla, V. (2003). Seismic geomorphology and stratigraphy of depositional elements in deep-water settings. Journal of sedimentary research, 73(3), 367-388. https://doi.org/10.1306/111302730367

Poyatos-Moré, M. (2014). Physical Stratigraphy and Facies Analysis of the Castissent Tecto-Sedimentary Unit. Universitat Autònoma de Barcelona. https://hdl.handle.net/10803/145397

Prélat, A., Hodgson, D. M., & Flint, S. S. (2009). Evolution, architecture and hierarchy of distributary deep-water deposits: a high-resolution outcrop investigation from the Permian Karoo Basin, South Africa. Sedimentology, 56(7), 2132-2154. https://doi.org/10.1111/j.1365-3091.2009.01073.x

Puigdefàbregas, C., & Souquet, P. (1986). Tecto-sedimentary cycles and depositional sequences of the Mesozoic and Tertiary from the Pyrenees. Tectonophysics, 129(1-4), 173-203. https://doi.org/10.1016/0040-1951(86)90251-9

Remacha, E., & Fernández, L. P. (2003). High-resolution correlation patterns in the turbidite systems of the Hecho Group (South-Central Pyrenees, Spain). Marine and Petroleum Geology, 20(6-8), 711-726. https://doi.org/10.1016/0040-1951(86)90251-9

Richardson, S. E., Davies, R. J., Allen, M. B., & Grant, S. F. (2011). Structure and evolution of mass transport deposits in the South Caspian Basin, Azerbaijan. Basin Research, 23(6), 702-719. https://doi.org/10.1016/0040-1951(86)90251-9

Rosenbaum, G., Lister, G. S., & Duboz, C. (2002). Relative motions of Africa, Iberia and Europe during Alpine orogeny. Tectonophysics, 359(1-2), 117-129. https://doi.org/10.1016/S0040-1951(02)00442-0

Salles, L., Ford, M., & Joseph, P. (2014). Characteristics of axially-sourced turbidite sedimentation on an active wedge-top basin (Annot Sandstone, SE France). Marine and Petroleum Geology, 56, 305-323. https://doi.org/10.1016/j.marpetgeo.2014.01.020

Sawyer, D. E., Flemings, P. B., & Nikolinakou, M. (2014). Continuous deep-seated slope failure recycles sediments and limits levee height in submarine channels. Geology, 42(1), 15-18. https://doi.org/10.1130/G34870.1

Sawyer, D. E., Flemings, P. B., Shipp, R. C., & Winker, C. D. (2007). Seismic geomorphology, lithology, and evolution of the late Pleistocene Mars-Ursa turbidite region, Mississippi Canyon area, northern Gulf of Mexico. AAPG bulletin, 91(2), 215-234. https://doi.org/10.1306/08290605190

Scotchman, J. I., Bown, P., Pickering, K. T., BouDagher-Fadel, M., Bayliss, N. J., & Robinson, S. A. (2015a). A new age model for the middle Eocene deep-marine Ainsa Basin, Spanish Pyrenees. Earth-Science Reviews, 144, 10-22. https://doi.org/10.1016/j.earscirev.2014.11.006

Sinclair, H. D. (2000). Delta-fed turbidites infilling topographically complex basins: a new depositional model for the Annot Sandstones, SE France. Journal of Sedimentary Research, 70(3), 504-519. https://doi.org/10.1306/2DC40923-0E47-11D7-8643000102C1865D

Smith, R., & Joseph, P. (2004). Onlap stratal architectures in the Gres d'Annot: geometric models and controlling factors. Geological Society, London, Special Publications, 221(1), 389-399. https://doi.org/10.1144/GSL.SP.2004.221.01.

Soutter, E. L., Bell, D., Cumberpatch, Z. A., Ferguson, R. A., Spychala, Y. T., Kane, I. A., & Eggenhuisen, J. T. (2021). The influence of confining topography orientation on experimental turbidity currents and geological implications. Frontiers in Earth Science, 8, 540633. https://doi.org/10.3389/feart.2020.540633

Soutter, E. L., Kane, I. A., Fuhrmann, A., Cumberpatch, Z. A., & Huuse, M. (2019). The stratigraphic evolution of onlap in siliciclastic deep-water systems: Autogenic modulation of allogenic signals. Journal of Sedimentary Research, 89(10), 890-917. https://doi.org/10.2110/jsr.2019.49

Soutter, E.L., Martínez-Doñate, A., Kane, I.A., Poyatos-Moré, M., Taylor, W., Hodgson, D.M., Bouwmeester, M.J. & Flint, S. (2023). Exceptional preservation of three-dimensional dunes on an ancient deep-marine seafloor: implications for sedimentary processes and depositional environments. EarthArXiv. https://doi.org/10.31223/X50D3P

Srivastava, S.P. and Roest, W.R. (1991). Roest, W. R., & Srivastava, S. P. (1991). Kinematics of the plate boundaries between Eurasia, Iberia, and Africa in the North Atlantic from the Late Cretaceous to the present. Geology, 19(6), 613-616. https://doi.org/10.1130/0091-7613(1991)019<0613:KOTPBB>2.3.CO;2

Stevenson, C. J., Jackson, C. A. L., Hodgson, D. M., Hubbard, S. M., & Eggenhuisen, J. T. (2015). Deep-water sediment bypass. Journal of Sedimentary Research, 85(9), 1058-1081. https://doi.org/10.2110/jsr.2015.63

Stevenson, C. J., Peakall, J., Hodgson, D. M., Bell, D., & Privat, A. (2020). TB or not TB: banding in turbidite sandstones. Journal of Sedimentary Research, 90(8), 821-842. https://doi.org/10.2110/jsr.2020.43

Steventon, M.J., Jackson, C.A.-L., Johnson, H.D., Hodgson, D.M., Kelly, S., Omma, J., Gopon, C., Stevenson, C. & Fitch, P. (2021). Evolution of a sand-rich submarine channel–lobe system, and the impact of mass-transport and transitional-flow deposits on reservoir heterogeneity: Magnus Field, Northern North Sea. Petroleum Geoscience, 27(3), petgeo2020-095. https://doi.org/10.1144/petgeo2020-095

Sumner, E. J., Amy, L. A., & Talling, P. J. (2008). Deposit structure and processes of sand deposition from decelerating sediment suspensions. Journal of Sedimentary Research, 78(8), 529-547. https://doi.org/10.2110/jsr.2008.062

Talling, P.J., Masson, D.G., Sumner, E.J. and Malgesini, G. (2012). Subaqueous sediment density flows: Depositional processes and deposit types. Sedimentology, 59(7), 1937-2003. https://doi.org/10.1111/j.1365-3091.2012.01353.x

Tek, D. E., McArthur, A. D., Poyatos-Moré, M., Colombera, L., Patacci, M., Craven, B., & McCaffrey, W. D. (2021). Relating seafloor geomorphology to subsurface architecture: How mass-transport deposits and knickpoint-zones build the stratigraphy of the deep-water Hikurangi Channel. Sedimentology, 68(7), 3141-3190. https://doi.org/10.1111/sed.12890

Tek, D. E., Poyatos-Moré, M., Patacci, M., McArthur, A. D., Colombera, L., Cullen, T. M., & McCaffrey, W. D. (2020). Syndepositional tectonics and mass-transport deposits control channelized, bathymetrically complex deep-water systems (Aínsa depocenter, Spain). Journal of Sedimentary Research, 90(7), 729-762. https://doi.org/10.2110/jsr.2020.38.

Terlaky, V., & Arnott, R. W. C. (2016). The control of terminal-splay sedimentation on depositional patterns and stratigraphic evolution in avulsion-dominated, unconfined, deep-marine basin-floor systems. Journal of Sedimentary Research, 86(7), 786-799. https://doi.org/10.2110/jsr.2016.51.

Thomson, K. D., Stockli, D. F., Clark, J. D., Puigdefàbregas, C., & Fildani, A. (2017). Detrital zircon (U-Th)/(He-Pb) double-dating constraints on provenance and foreland basin evolution of the Ainsa Basin, south-central Pyrenees, Spain. Tectonics, 36(7), 1352-1375. https://doi.org/10.1002/2017TC004504.

Tinterri, R. (2011). Combined flow sedimentary structures and the genetic link between sigmoidal-and hummocky-cross stratification. GeoActa, 10(4), 1-43.

Tinterri, R., Laporta, M., & Ogata, K. (2017). Asymmetrical cross-current turbidite facies tract in a structurally-confined mini-basin (Priabonian-Rupelian, Ranzano Sandstone, northern Apennines, Italy). Sedimentary Geology, 352, 63-87. https://doi.org/10.1016/j.sedgeo.2016.12.005.

Tinterri, R., & Magalhaes, P. M. (2011). Synsedimentary structural control on foredeep turbidites: An example from Miocene Marnoso-arenacea Formation, Northern Apennines, Italy. Marine and Petroleum Geology, 28(3), 629-657. https://doi.org/10.1016/j.marpetgeo.2010.07.007.

Valdez. V., Milana, J. P., Sobiesiak, M. S., & Kneller, B. (2019). The Carboniferous MTD Complex at La Peña Canyon, Paganzo Basin (San Juan, Argentina). Submarine landslides: subaqueous mass transport deposits from outcrops to seismic profiles, 105-116. https://doi.org/10.1002/9781119500513.ch7.

Van Toorenenburg, K. A., Donselaar, M. E., Noordijk, N. A., & Weltje, G. J. (2016). On the origin of crevasse-splay amalgamation in the Huesca fluvial fan (Ebro Basin, Spain): Implications for connectivity in low net-to-gross fluvial deposits. Sedimentary Geology, 343, 156-164. https://doi.org/10.1016/j.sedgeo.2016.08.008

Zhong, G., & Peng, X. (2021). Transport and accumulation of plastic litter in submarine canyons—The role of gravity flows. Geology, 49(5), 581-586. https://doi.org/10.1130/G48536.1.

How to cite: Martinez-Doñate, A., Soutter, E. L., Kane, I. A., Poyatos-Moré, M., Hodgson, D. M., Ayckbourne, A. J. M., Taylor, W. J., Bouwmeester, M. J., & Flint, S. S. (2023). Submarine crevasse lobes controlled by lateral slope failure in tectonically-active settings: an exhumed example from the Eocene Aínsa depocentre (Spain). Sedimentologika, 1(1), 1-25. https://doi.org/10.57035/journals/sdk.2023.e11.1068